AWARD NUMBER: W81XWH-12-1-0179

TITLE: Unbiased Combinatorial Genomic Approaches to Identify Alternative Therapeutic Targets within the TSC Signaling Network

PRINCIPAL INVESTIGATOR: Norbert Perrimon

CONTRACTING ORGANIZATION: Harvard University
Boston, MA 02115

REPORT DATE: September 2015

TYPE OF REPORT: Final

PREPARED FOR: U.S. Army Medical Research and Materiel Command
Fort Detrick, Maryland 21702-5012

REPORT DOCUMENTATION PAGE

Form Approved
OMB No. 0704-0188

1. REPORT DATE	2. REPORT TYPE	3. DATES COVERED
September 2015	Final	1June2012 - 31May2015

4. TITLE AND SUBTITLE
Unbiased Combinatorial Genomic Approaches to Identify

Alternative Therapeutic Targets within the TSC Signaling

Network

5a. CONTRACT NUMBER
W81XWH-12-1-0179

5b. GRANT NUMBER

5c. PROGRAM ELEMENT NUMBER

6. AUTHOR(S)
Dr. Norbert Perrimon and Dr. Brendan Manning

E-Mail: perrimon@receptor.med.harvard.edu

5d. PROJECT NUMBER

5e. TASK NUMBER

5f. WORK UNIT NUMBER

7. PERFORMING ORGANIZATION NAME(S) AND ADDRESS(ES)

Harvard University
Sponsored Programs Admin
25 Shattuck Street
Boston, MA 02115-6027

8. PERFORMING ORGANIZATION REPORT NUMBER

9. SPONSORING / MONITORING AGENCY NAME(S) AND ADDRESS(ES)

U.S. Army Medical Research and Materiel Command
Fort Detrick, Maryland 21702-5012

10. SPONSOR/MONITOR'S ACRONYM(S)

11. SPONSOR/MONITOR'S REPORT NUMBER(S)

12. DISTRIBUTION / AVAILABILITY STATEMENT

Approved for Public Release; Distribution Unlimited

13. SUPPLEMENTARY NOTES

14. ABSTRACT

The goal of this project was to identify robust synthetic lethal interactions between TSC and kinases and phosphatases by taking advantage of the evolutionary conservation of the pathway. We first identified such interactions in Drosophila cells and tested the candidates in TSC human patient cells. We identified three hits (mRNA-Cap, Pitslre and CycT) that scored as synthetic lethal with both TSC1 and TSC2 mutations in Drosophila and validated the mammalian orthologs of the three hits as having synthetic lethal relationships with TSC2 in both mouse and human cells, as their depletion selectively decreases the viability of TSC2 null cells. These candidates are now strong drug candidates for TSC.

15. SUBJECT TERMS
Drosophila, TSC, Drug Targets, Combinatorial Screen, Cancer

16. SECURITY CLASSIFICATION OF:			17. LIMITATION OF ABSTRACT	18. NUMBER OF PAGES	19a. NAME OF RESPONSIBLE PERSON
a. REPORT	b. ABSTRACT	c. THIS PAGE			USAMRMC
U	U	U	UU	86	19b. TELEPHONE NUMBER *(include area code)*

Table of Contents

Page

1. INTRODUCTION:

A detailed understanding of how common oncogenic signaling pathways are assembled into larger signaling networks is essential to developing therapeutic strategies to properly target these pathways in cancer and for interpreting clinical outcomes from targeted therapeutics. While the effected oncogenes and tumor suppressors that predominate different classes of human cancer can vary greatly, a small number of highly integrated signaling nodes are affected in the majority of human cancers, regardless of tissue of origin. It is therefore important to understand how these key signaling nodes are regulated. In this project, we focus on one such node, involving the TSC1-TSC2 complex and the Ras related small G protein Rheb, which is aberrantly regulated in nearly all genetic tumor syndromes and the most common forms of sporadic cancer. The long-term goal of this project is geared toward further defining the regulatory mechanisms impinging on the TSC-Rheb circuit and revealing therapeutic strategies to target this signaling network in genetic tumor syndromes and cancer. For this purpose, we have used high-throughput technologies in *Drosophila* to identify synthetic lethal interactions between TSC network tumor suppressors and identified pathway interactors. We then went on to validate positive hits in an *in vivo Drosophila* model before determining which interactions were conserved using mammalian cell culture.

2. KEYWORDS:

Drosophila, TSC, Drug Targets, Combinatorial Screen, Cancer

3. OVERALL PROJECT SUMMARY:

We have made progress towards all the initial goals. Details are provided below according to the original Statement of Work:

Task 1. Establish a robust synthetic lethal screening method applied to the study of the TSC network. (months 1-36).

- Characterize an optimized shRNA targeting each of the core tumor suppressors. (months 1-2) COMPLETED
- Characterize the tumor suppressor genomic rescue constructs. (months 1-2) COMPLETED
- Clone shRNAs targeting each of the candidate genes into each of these constructs to create the desired pairwise combinations. (months 3-8) COMPLETED
- Establish tumor suppressor cell lines (months 12-24) COMPLETED
- Perform the synthetic screen for viability with kinase and phosphatase set (months 8-14) COMPLETED
- Confirm the positives (months 14-24) COMPLETED
- Perform more quantitative screens using phospho-AKT, dpERK, and phospho-S6K antibodies (months 24-36) COMPLETED

-Expand the synthetic lethal screen to the Insulin network (months 24-36) COMPLETED

In order to perform robust combinatorial screens we have developed a novel method combining dsRNA screens in CRISPR generated TSC1 and TSC2 mutant cell lines. Specifically, we combined the CRISPR genome editing system with a novel approach allowing efficient single cell cloning of *Drosophila* cells with the aim of generating knockout cell lines for five tumor suppressors (TSC1, TSC2/gig, Nf1, Lkb1 and Pten) within the TSC/Insulin signaling pathway (Housden et al., Science Signaling. In press).

To enable the use of the CRISPR system to generate mutant cell lines, we first assessed the specificity of mutation in *Drosophila* S2R+ cells. We generated a quantitative mutation reporter vector in which an sgRNA target sequence was cloned into the coding sequence of the luciferase gene immediately following the start codon. A fixed proportion of indels induced by the CRISPR system at this site therefore lead to frame shift of the luciferase gene and ablation of functional protein. 75 sgRNA expressing plasmids were generated with varying number and position of mismatches to the target sequence and cotransfected into S2R+ cells with the reporter construct and luciferase levels measured after 4 days to determine mutation rate. From this analysis, we found that 3bp of mismatch is sufficient to prevent detectible mutation as long as at least 1 mismatch is within the 15bp 3' seed region (Figure 1A). Importantly, this result demonstrates high specificity compared to mammalian systems where mutations have been detected with 5bp of mismatch.

Next, we tested whether sgRNA efficiency could be predicted based on sequence. Previous experiments have demonstrated widely varying mutation rates between sgRNAs so a method of predicting efficiency would greatly facilitate the use of CRISPR to generate mutant cell lines. To achieve this, we generated luciferase reporters similar to that described above, containing 75 different target sequences and corresponding sgRNA expressing plasmids for each. Previous reports have suggested that high GC content at the 3' end of the sgRNA is associated with high efficiency yet our results contradict this with no evident correlation (Figure 1B). We analyzed the base pair composition of each position amongst high and low efficiency sgRNAs from the 75 that we tested. From this, we were able to generate a matrix representing the

association of each base in each position within the sgRNA with high mutation rate (Figure 1C) and generate a sequence-based scoring algorithm to predict efficiency. Comparison with independent data from two *Drosophila* publications showed good correlation between the scores we generated and the reported mutation rates (Figure 1D).

Although CRISPR works with high efficiency in cultured *Drosophila* cells, previous attempts to generate mutant *Drosophila* cell lines using CRISPR have failed due to rapid selection for wildtype cells and reversion of the population. We therefore tested whether it would be possible to isolate single mutant cells and culture these to produce cultures completely lacking wildtype sequence at the target locus. No robust methods existed to clone single *Drosophila* cells so we tested an approach where single cells isolated using flow cytometry were seeded into different media formulations. We found that the use of preconditioned media allowed robust survival and expansion of single S2R+ cells in culture (Figure 2A).

Next, we tested whether a CRISPR-treated population contained single cells lacking wildtype sequence (homozygous mutations). 30 single cells were tested using high-resolution melt assays (HRMA) and 21 were identified as carrying mutations. 8 of these were sequenced and wild type sequences were absent from all of them (Figure 2B and data not shown), indicating that the generation of mutant cell lines using this method was likely to be efficient (Figure 2C).

We have successfully produced mutant lines for three of the tumor suppressor genes (Nf1, TSC1 and gig/TSC2). We also attempted to generate mutant lines for Lkb1 and Pten although severely reduced proliferation rates prevented the maintenance of these cells.

Characterization of the mutant cell lines demonstrated that the observed morphological and cell growth phenotypes are consistent with previously demonstrated in vivo phenotypes (Figure 3). Additionally, we performed phosphoproteome analysis of TSC1 and gig/TSC2 mutant lines and the identified changes in phosphorylation were broadly consistent with known targets of the TSC complex, indicating that these cell lines are a good model of the TSC signaling network. Furthermore, we performed combinatorial screens by treating the mutant lines with dsRNAs targeting all kinases and phosphatases (563 genes) in the *Drosophila* genome (Figure 4). 65 samples that displayed synthetic lethality (15 genes) or synthetic increases in viability (50 genes) with TSC1 and/or gig/TSC2 mutations were selected as hits (Figure 4), three of which scored as synthetic lethal with both TSC1 and gig/TSC2 mutations (mRNA-Cap, Pitslre and CycT). Interestingly, mRNA-Cap is required for the addition of 7-methylguanosine caps to mRNA molecules. This cap is the target of 4EBP regulation downstream of insulin signaling, indicating a likely mechanism for the observed synthetic lethality.

Task 2: Validation of synthetic lethal pairs in an *in vivo* intestinal stem cell system. (months 1-36).

- Characterize the phenotypes and level of knockdown of single shRNAs targeting the five tumor suppressors in ISCs. (months 1-6) COMPLETED
- Characterize shRNAs targeting each gene that show synthetic phenotypes in combinations with the tumor suppressors. (months 6-24) COMPLETED
- Characterize in details the phenotypes of the synthetic interactions using phosphoHistone H3, caspase antibodies, and BrDU. (months 12-36) UNDERWAY
- Characterize in further details the phenotypes of the synthetic interactions using pathway specific phospho-antibodies such as phospho-AKT, dpERK, and phospho-S6K (months 14-36) COMPLETED
- Confirm by genomic rescue the specificity of the interactions (months 15-36). COMPLETED

We have made excellent progress at characterizing the phenotype of tumor suppressor in gut stem cells. Specifically, we have shown that single knockdowns of *PTEN*, *AMPK*, *TSC1*, or *TSC2* in *Drosophila* adult gut intestinal stem stems (ISCs), via expression of shRNAs from an ISC-specific promoter (esg), lead to the rapid generation of hyperproliferative lesions/tumors (**Figure 5A**). In addition, we have developed a blood cell assay that will allow us to examine the effect of shRNA combinations on blood cell proliferation (**Figure 5B).** These assays will be used to validate the synthetic lethal pairs that have emerged from Task 1.

Task 3: Determine whether synthetic lethal combinations found in *Drosophila* are relevant to mammalian networks. (months 1-36)

- Characterize the signaling and growth properties of the knockout MEFs for all of the five major tumor suppressor genes of interest (LKB1, NF1, PTEN, TSC1, and TSC2). (months 1-8) COMPLETED
- Identify the mammalian orthologs using DIOPT. (months 8-30) COMPLETED
- Characterize effective siRNAs against the genes to be targeted using ON-TARGETplus SMARTpool siRNAs from Dharmacon. (months 12-30) COMPLETED
- Test the synthetic lethal interactions with the RTK network core tumor suppressors in MEFs. (months 12-30) COMPLETED
- Confirm the results with neutral base pair substitutions control siRNAs. (months 12-30) UNDERWAY
- Test hits that show specificity for killing of one or more tumor suppressor-deficient cell types using available tumor-derived cell lines lacking these tumor suppressors. (months 26-36) COMPLETED
- Test all synthetic lethal interactions, regardless of the MEF results, in a TSC2 null angiomyolipoma-derived cell line. (months 26-36) COMPLETED

With the *Drosophila* TSC1 and TSC2 knockout lines generated and the synthetic lethal screens completed, we then tested the hits in mammalian cell lines. We used the DIOPT software to identify the human orthologs of the high confidence hits from the synthetic lethal screen. The identified orthologs were: 1) RNGTT (mRNA-CAP), which is the RNA guanyltransferase and 5'-phosphatase that initiates the capping of mRNAs; 2) CDK11B (Pitslre), a member of the cyclin-dependent kinase family implicated in the control of both mitosis and autophagy; 3) CCNT1 (CycT), a cyclin family member that, through its association with CDK9, forms the P-TEFb complex involved in mRNA maturation during RNA pol II-mediated transcription. We tested whether the synthetic interactions between *mRNA-cap, Pitslre* and *CycT* and *TSC1* and *TSC2* were conserved by using siRNAs targeting each of the three genes in $TSC2^{-/-}$ MEFs compared to littermate-derived $TSC2^{+/+}$ MEFs. Both *RNGTT* and *CCNT1* knockdowns caused reduced population growth in $TSC2^{-/-}$ cells compared to $TSC2^{+/+}$ (**Figure 6**). No synthetic effect was detected with *CDK11* because *CDK11* knockdown caused reduced mTORC1 activity in both the $TSC2^{+/+}$ and $TSC2^{-/-}$ MEFs. Next, we used siRNAs to knockdown the three hits in a *TSC2*-deficient human renal angiomyolipoma (AML) cell line derived from a patient with LAM (Figure 7). The same cell line stably reconstituted with wild-type TSC2 was used as a control. siRNAs targeting each of the three hits specifically reduced the population growth of *TSC2* null cells (**Figure 7**). In addition, synthetic effects were seen on cell numbers for all three genes, indicating that the three gene products we have identified are promising drug targets for TSC treatment. The final remaining item that is underway is to further validate these hits by re-expressing RNAi-resistant cDNAs encoding these targets.

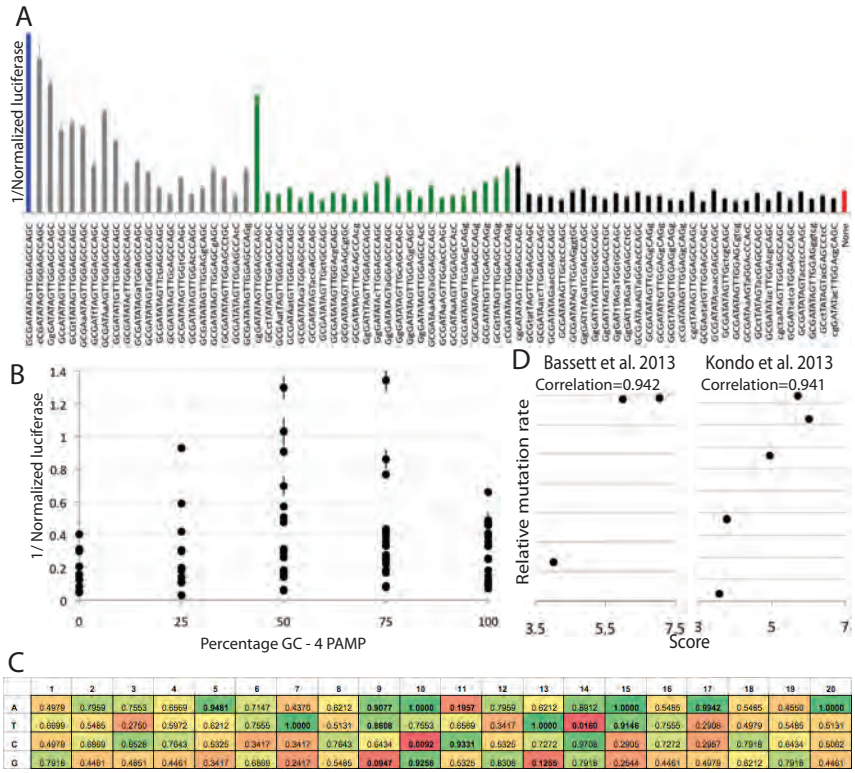

	1	2	3	4	5	6	7	8	9	10	11	12	13	14	15	16	17	18	19	20
A	0.4979	0.7959	0.7553	0.6869	0.9481	0.7147	0.4376	0.8212	0.9077	1.0000	0.1957	0.7959	0.6212	0.8912	1.0000	0.5485	0.9342	0.5485	0.4559	1.0000
T	0.6899	0.5485	0.2750	0.5972	0.8212	0.7555	1.0000	0.5131	0.8608	0.7553	0.6569	0.3417	1.0000	0.0166	0.9146	0.7555	0.2906	0.4979	0.5485	0.5131
C	0.4979	0.6869	0.6528	0.7643	0.5326	0.3417	0.3417	0.7643	0.6434	0.0092	0.9331	0.5326	0.7272	0.9708	0.2905	0.7272	0.2967	0.7918	0.6434	0.5082
G	0.7918	0.4461	0.4851	0.4461	0.3417	0.6869	0.2417	0.5485	0.0947	0.0258	0.5326	0.8306	0.1259	0.7918	0.2644	0.4461	0.4979	0.8212	0.7918	0.4461

Figure 1: Optimization of the CRISPR system for use in Drosophila S2R+ cells

A: The graph shows 1/normalized luciferase luminescence to represent relative mutation efficiency for the 75 gRNAs shown on the horizontal axis. The blue bar shows a positive control with a perfect match between the sgRNA and the target sequence. Gray, blue and black bars show sgRNAs with 1, 2 or 3-6 mismatches respectively with varying position within the sequence. The red bar shows a negative control in which no sgRNA was present. B: The scatter plot shows 1/normalized luciferase luminescence (mutation efficiency) on the vertical axis and the percentage GC content in the 4bp proximal to the PAM sequence of the 75 sgRNAs shown. All sgRNAs in this experiment are perfect matches to their respective target sites. C: The results shown in B were used to assess the association of nucleotide content in each position of the 75 sgRNAs with high mutation efficiency. These data were then used to produce the probability matrix shown. Numbers represent the p-value associated with each base in each position leading to high mutation efficiency defined by >50% of maximum efficiency shown in B. D: The matrix shown in C was sued to generate a sequence-based scoring algorithm to predict sgRNA efficiency. To validate this, scores were generated for sgRNA sequences with published mutation efficiencies from two independent studies. In both cases, a strong correlation is observed between score and reported efficiency. Note that sgRNAs from these studies that were unlikely to have representative mutation efficiencies due to position within the target gene or reduced viability were not included in this analysis.

A

Media		Clones	% survival
Schneider's	10% FBS	0	0.0
	15% FBS	0	0.0
	20% FBS	0	0.0
Conditioned Schneider's	10% FBS	30	15.8
	15% FBS	31	16.3
	20% FBS	32	16.8

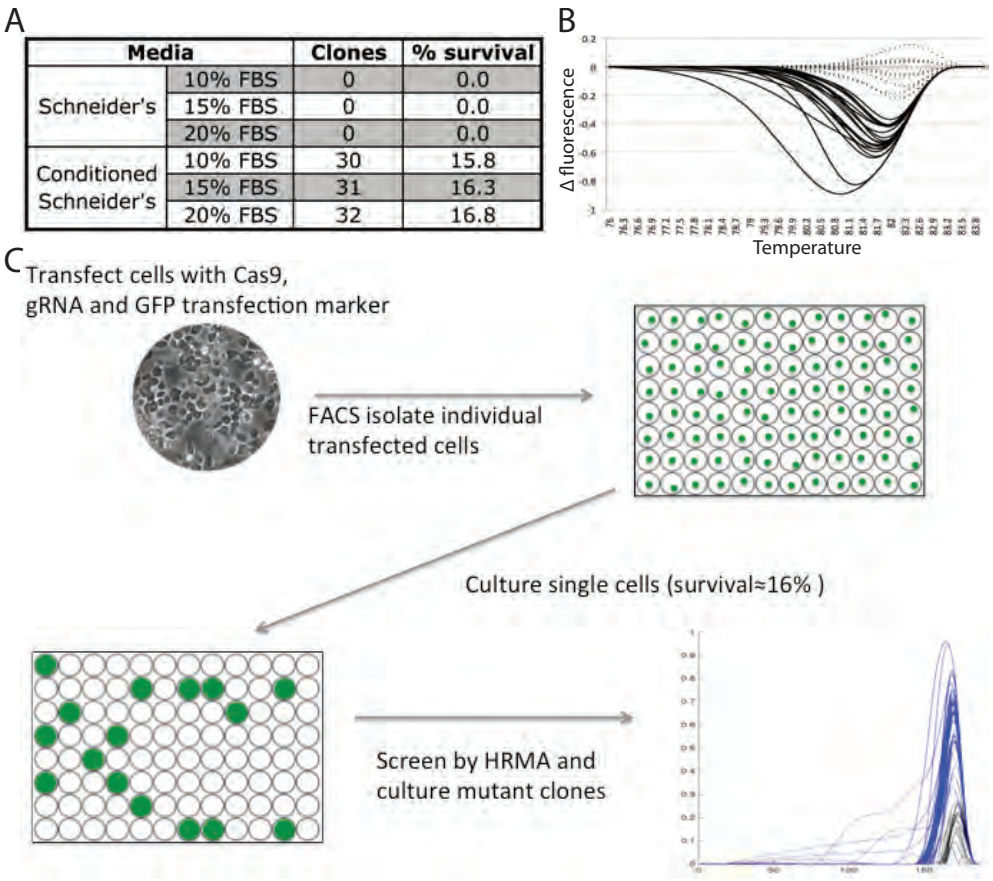

Figure 2: A method to generate stable, homogeneous mutant S2R+ cell lines
A: Several culture media variations were tested to find conditions allowing single cell cloning of S2R+ cells. The table shows the survival rate of single cell clones under 6 different conditions. Conditioned media was produced by culturing wildtype S2R+ cells in fresh media for 16 hours. Cells were then removed by filtration to isolate conditioned media. B: HRMA assays were used to detect single cells from a CRISPR-treated population that carried mutations of the target site. Black lines represent cells differing significantly from controls and dashed lines represent samples that do not differ significantly from controls and are therefore unlikely to carry mutations. C: Schematic of the approach to combine CRISPR-based genome editing and single cell cloning to generate mutant cell lines.

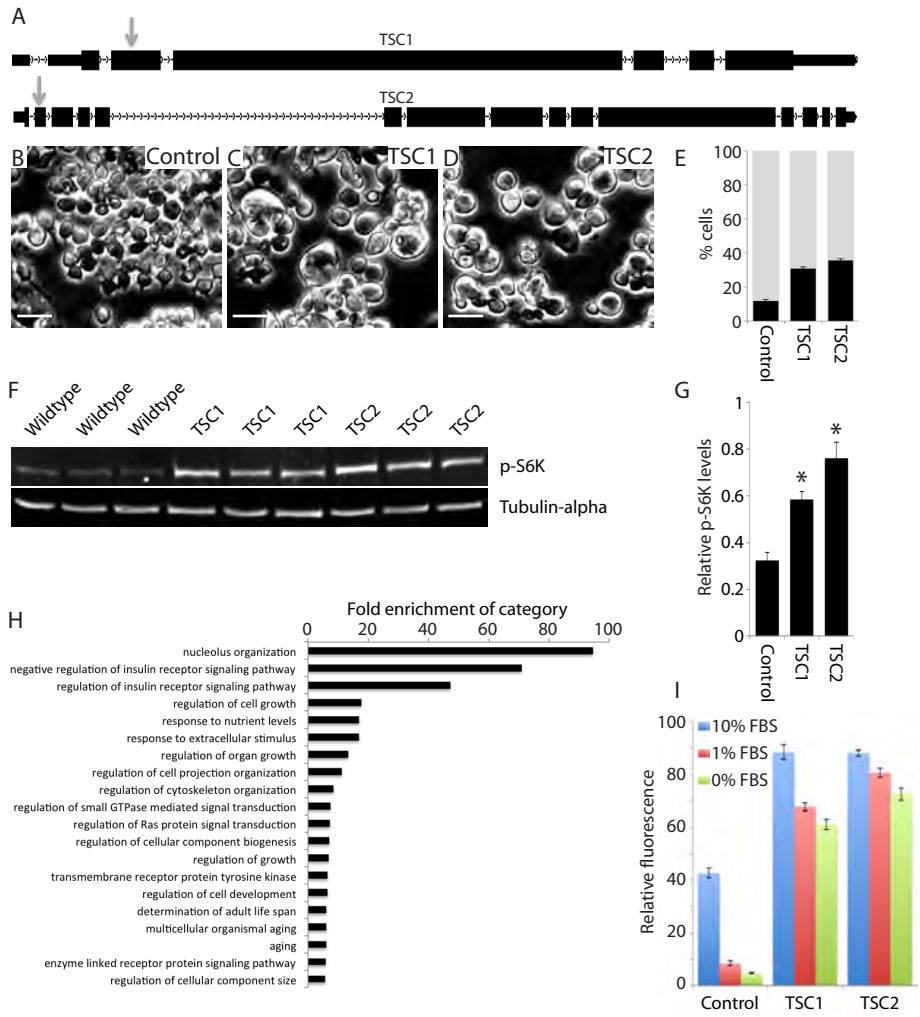

Figure 3: Characterization of Tsc1 and gig/Tsc2 mutant cell lines

A: Schematic indicating the site of mutation in the TSC1 and gig/TSC2 genes. B-D: Images of wild type, TSC1 mutant and gig/TSC2 mutant cells illustrating an increase in cell size as expected from known phenotypes for these genes. E: Quantification of cell size distribution for each cell line. Black bars indicate the proportion of cells with diameter over an arbitrary threshold. Gray bars indicate the proportion of cells under the same diameter threshold. F: Western blot indicating levels of phosphorylated S6k in wildtype, TSC1 or gig/TSC2 cells. G: Quantification of phosphorylated S6k levels relative to Tubulin-alpha as shown in F. H: Enriched GO terms from proteins differentially phosphorylated in TSC1 and gig/TSC2 cells compared to wildtype cells. I: The population growth rates of each cell type were measured after 4 days of culture using CellTitre Glo assays under normal culture conditions (blue bars) or under serum starvation conditions (red bars – partial starvation and green bars – complete starvation). Results show that the mutant cell lines are no longer responsive to changes in the nutrient status of the culture media.

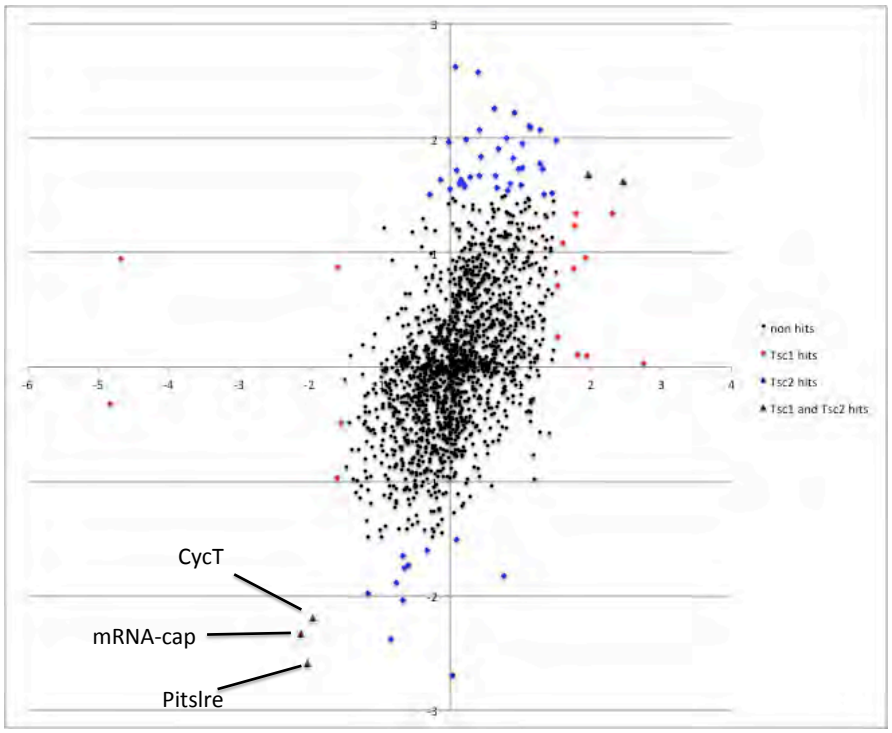

Figure 4: Synthetic screening results
The scatter plot displays Z-scores from the screens in TSC1 and gig/TSC2 mutant cell lines. Samples that displayed significant changes in viability in wild type cells are not shown. The three genes that have synthetic lethal relationships with both TSC1 and gig/TSC2 are indicated.

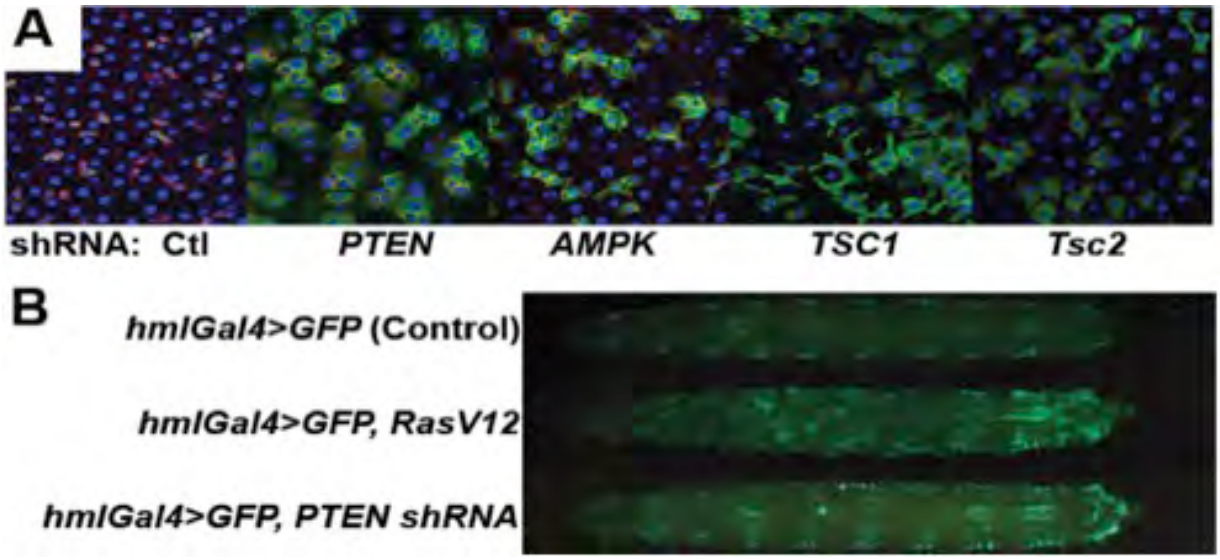

Figure 5: In vivo assays
A: As in mammals, fly ISCs divide about once a day to maintain themselves and produce daughter cells (marked by esg-GFP in green) that differentiate into enterocytes (large blue nuclei). Upon shRNA-knockdown of *PTEN*, *AMPK*, or *TSC1/2* in ISCs (esg-Gal4;UAS-geneX-RNAi), ISCs proliferate and develop "gut tumors" within three days, detectable by GFP. B: Coexpression of RasV12 or PTEN shRNAs with GFP using the hemolectin (hml)-Gal4 driver demonstrates increase larval blood cell proliferation.

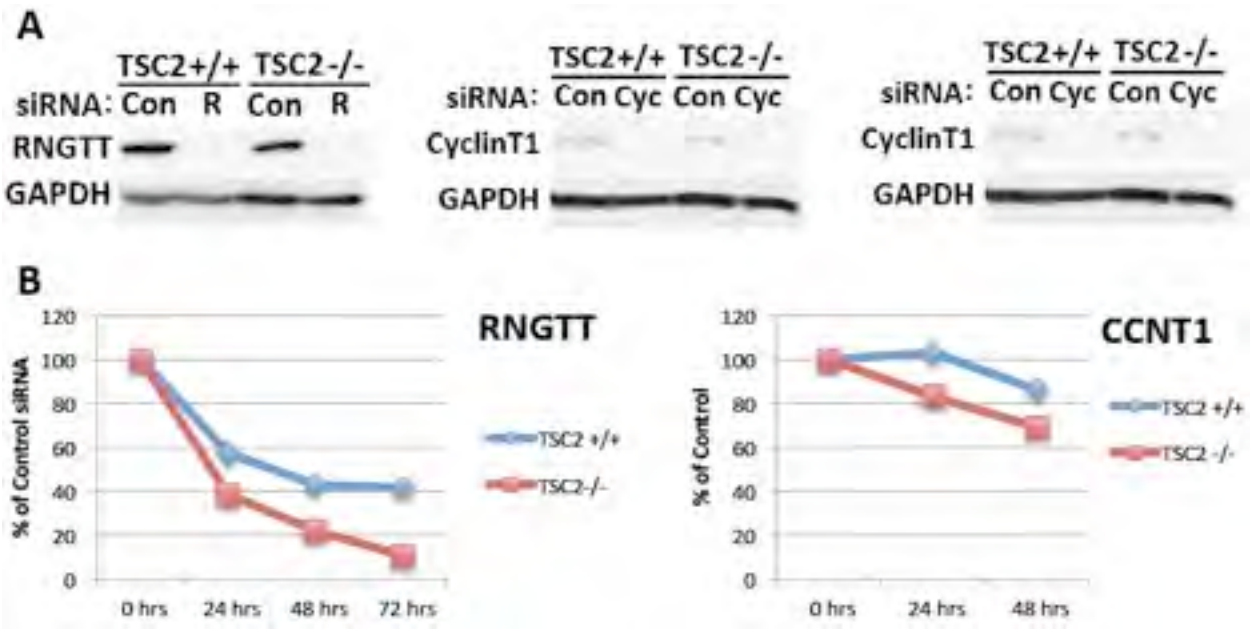

Figure 6: Validation of hits from *Drosophila* synthetic lethal screen in mouse embryo fibroblasts (MEFs). (A) The most effective siRNAs against the three targets identified in the *Dropsophila* genetic screen are shown, demonstrating strong knockdown of the mammalian orthologs by immunoblot with available antibodies. (B) The effects of these siRNAs on the viability of *Tsc2+/+* versus *Tsc2-/-* MEFs are shown, measured by Cell-Titer Glo and normalized to each cell line transfected with control, non-targetting siRNAs.

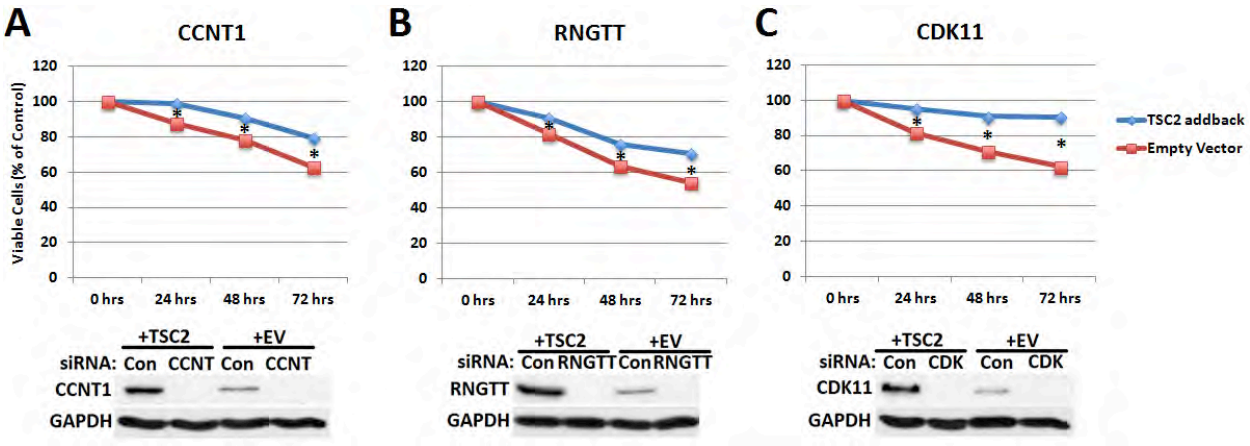

Figure 7: Validation of hits from *Drosophila* synthetic lethal screen in angiomyolipoma cells. Patient-derived *TSC2*-deficient angiomyolipoma cells were stably transfected with wild type human TSC2 (TSC2 addback) or Empty Vector. Cells then received control (scrambled), CCNT1, RNGTT, or CDK11 siRNA and viable cells were quantified every 24 hrs using the Cell Titer Glo Cell Viability Assay. Data shown are an average of 3 independent experiments each done in triplicate, represented as percent of the control siRNA treated cells. *$p<0.03$. Efficient knockdown of all 3 targets was confirmed in both cell lines by western blot.

4. KEY RESEARCH ACCOMPLISHMENTS:

. Successfully produced mutant cell lines for three of the tumor suppressor genes (Nf1, TSC1 and gig/TSC2)

. Successfully performed combinatorial screens by treating the mutant lines with dsRNAs targeting all kinases and phosphatases (563 genes) in the *Drosophila* genome.

. Identified three hits (mRNA-Cap, Pitslre and CycT) that scored as synthetic lethal with both TSC1 and gig/TSC2 mutations.

. Validated the mammalian orthologs of the three hits as having synthetic lethal relationships with TSC2 in both mouse and human cells, as their depletion selectively decreases the viability of TSC2 null cells, making them strong drug candidates for TSC.

5. CONCLUSION:

The tuberous sclerosis complex (TSC) tumor suppressors, TSC1 and TSC2, function together in an evolutionarily conserved protein complex that is a point of convergence for major cell signaling pathways regulating mTOR complex 1 (mTORC1). Mutation or aberrant inhibition of TSC is common in a diverse array of human tumor syndromes and cancers across tissue lineages. The discovery of novel therapeutic strategies to selectively kill cells with functional loss of this complex is therefore of significant clinical relevance. We have developed a CRISPR-based method allowing the generation of homogeneous mutant *Drosophila* cell lines. By combining *TSC1* and *TSC2* mutant cell lines with RNAi screens against all kinases and phosphatases, we identified synthetic lethal interactions with *TSC1* and *TSC2*. Knockdown of three genes (mRNA-cap/RNGTT, CycT/CCNT1, Pitslre/CDK11) reduced viability of both *Drosophila TSC1* and *TSC2* mutant cells but left wild type cells unaffected. Importantly, knockdown of these genes displayed similar selective viability effects in mammalian TSC2-deficient cell lines, including tumor-derived cell lines from a TSC patient, illustrating the power of this cross species screening strategy to identify new drug targets. The long-term impact of these studies is to identify drug targets for treating patients with TSC tumors.

6. PUBLICATIONS, ABSTRACTS, AND PRESENTATIONS:

Housden BE, Valvezan AJ, Kelley C, Sopko R, Lin S, Hu Y, Roesel C, Buckner M, Tao R, Yilmazel B, Mohr S, Manning BD, Perrimon N. Identification of novel drug targets for Tuberous Sclerosis Complex by synthetic screens combining CRISPR-based knockouts with RNAi. **Science Signaling.** In press.

7. INVENTIONS, PATENTS AND LICENSES:

Provisional patent application: Compositions and methods for inhibiting cell proliferation

8. REPORTABLE OUTCOMES:

Nothing to report.

9. OTHER ACHIEVEMENTS:

Nothing to report.

10. REFERENCES:

Barry ER, Morikawa T, Butler BL, Shrestha K, de la Rosa R, Yan KS, et al. Restriction of intestinal stem cell expansion and the regenerative response by YAP. Nature. 2013;493(7430):106-10.

Briggs AW, Rios X, Chari R, Yang L, Zhang F, Mali P, et al. Iterative capped assembly: rapid and scalable synthesis of repeat-module DNA such as TAL effectors from individual monomers. Nucleic Acids Res. 2012;40(15):e117.

Cermak T, Doyle EL, Christian M, Wang L, Zhang Y, Schmidt C, et al. Efficient design and assembly of custom TALEN and other TAL effector-based constructs for DNA targeting. Nucleic Acids Res. 2011;39(12):e82.

Charpentier E, Doudna JA. Biotechnology: Rewriting a genome. Nature. 2013;495(7439):50-1.

Cho SW, Kim S, Kim JM, Kim JS. Targeted genome engineering in human cells with the Cas9 RNA-guided endonuclease. Nat Biotechnol. 2013;31(3):230-2.

Cong L, Ran FA, Cox D, Lin S, Barretto R, Habib N, et al. Multiplex genome engineering using CRISPR/Cas systems. Science. 2013;339(6121):819-23.

Dahlem TJ, Hoshijima K, Jurynec MJ, Gunther D, Starker CG, Locke AS, et al. Simple methods for generating and detecting locus-specific mutations induced with TALENs in the zebrafish genome. PLoS Genet. 2012;8(8):e1002861.

Gratz SJ, Cummings AM, Nguyen JN, Hamm DC, Donohue LK, Harrison MM, et al. Genome engineering of Drosophila with the CRISPR RNA-guided Cas9 nuclease. Genetics. 2013.

Housden, B. E., Lin, S., Hu, Y., Flockhart, I., Roesel, C., Kelley, C., Buckner, M., Tao, R., Yilmazel, B., Mohr, S., and Perrimon, N. (2014). Generation of clonal *Drosophila* mutant cell lines. Submitted.

Liu J, Li C, Yu Z, Huang P, Wu H, Wei C, et al. Efficient and specific modifications of the Drosophila genome by means of an easy TALEN strategy. J Genet Genomics. 2012;39(5):209-15.

Hwang WY, Fu Y, Reyon D, Maeder ML, Tsai SQ, Sander JD, et al. Efficient genome editing in zebrafish using a CRISPR-Cas system. Nat Biotechnol. 2013;31(3):227-9.

Hockemeyer D, Wang H, Kiani S, Lai CS, Gao Q, Cassady JP, et al. Genetic engineering of human pluripotent cells using TALE nucleases. Nat Biotechnol. 2011;29(8):731-4.

Karpowicz P, Perez J, Perrimon N. The Hippo tumor suppressor pathway regulates intestinal stem cell regeneration. Development. 2010;137(24):4135-45.

Lin G, Xu N, Xi R. Paracrine Wingless signalling controls self-renewal of Drosophila intestinal stem cells. Nature. 2008;455(7216):1119-23.

Mali P, Yang L, Esvelt KM, Aach J, Guell M, DiCarlo JE, et al. RNA-guided human genome engineering via Cas9. Science. 2013;339(6121):823-6.

Markstein M, Pitsouli C, Villalta C, Celniker SE, Perrimon N. Exploiting position effects and the gypsy retrovirus insulator to engineer precisely expressed transgenes. Nat Genet. 2008;40(4):476-83.

Micchelli CA, Perrimon N. Evidence that stem cells reside in the adult Drosophila midgut

epithelium. Nature. 2006;439(7075):475-9.

Moore FE, Reyon D, Sander JD, Martinez SA, Blackburn JS, Khayter C, et al. Improved somatic mutagenesis in zebrafish using transcription activator-like effector nucleases (TALENs). PLoS One. 2012;7(5):e37877.

Ohlstein B, Spradling A. The adult Drosophila posterior midgut is maintained by pluripotent stem cells. Nature. 2006;439(7075):470-4.

Ohlstein B, Spradling A. Multipotent Drosophila intestinal stem cells specify daughter cell fates by differential notch signaling. Science. 2007;315(5814):988-92.

Radtke F, Clevers H. Self-renewal and cancer of the gut: two sides of a coin. Science. 2005;307(5717):1904-9.

Reyon D, Tsai SQ, Khayter C, Foden JA, Sander JD, Joung JK. FLASH assembly of TALENs for high-throughput genome editing. Nat Biotechnol. 2012;30(5):460-5.

Sanjana NE, Cong L, Zhou Y, Cunniff MM, Feng G, Zhang F. A transcription activator-like effector toolbox for genome engineering. Nat Protoc. 2012;7(1):171-92.

Zu Y, Tong X, Wang Z, Liu D, Pan R, Li Z, et al. TALEN-mediated precise genome modification by homologous recombination in zebrafish. Nat Methods. 2013;10(4):329-31.

11. APPENDICES:

Housden BE, Valvezan AJ, Kelley C, Sopko R, Lin S, Hu Y, Roesel C, Buckner M, Tao R, Yilmazel B, Mohr S, Manning BD, Perrimon N. Identification of novel drug targets for Tuberous Sclerosis Complex by synthetic screens combining CRISPR-based knockouts with RNAi. **Science Signaling.** In press.

Identification of potential drug targets for Tuberous Sclerosis Complex by synthetic screens combining CRISPR-based knockouts with RNAi

Authors: Benjamin E. Housden[1*], Alexander J. Valvezan[2], Colleen Kelley[1], Richelle Sopko[1], Yanhui Hu[1], Charles Roesel[1], Shuailiang Lin[1], Michael Buckner[1], Rong Tao[1], Bahar Yilmazel[1], Stephanie Mohr[1], Brendan D. Manning[2] and Norbert Perrimon[1,3*]

Affiliations:

[1] Department of Genetics, Harvard Medical School, Boston, MA, 02115

[2] Department of Genetics and Complex Diseases, Harvard School of Public Health, Boston, MA, 02115

[3] Howard Hughes Medical Institute, 77 Avenue Louis Pasteur, Boston, MA, 02115

*Correspondence to:

Benjamin E. Housden bhousden@genetics.med.harvard.edu and

Norbert Perrimon perrimon@receptor.med.harvard.edu

Abstract

The tuberous sclerosis complex (TSC) family of tumor suppressors, TSC1 and TSC2, function together in an evolutionarily conserved protein complex that is a point of convergence for major cell signaling pathways that regulate mTOR complex 1 (mTORC1). Mutation or aberrant inhibition of the TSC complex is common in various human tumor syndromes and cancers. The discovery of novel therapeutic strategies to selectively target cells with functional loss of this complex is therefore of clinical relevance to patients with non-malignant tuberous sclerosis complex and those with sporadic cancers. We developed a CRISPR-based method to generate homogenous mutant *Drosophila* cell lines. By combining *TSC1* or *TSC2* mutant cell lines with RNAi screens against all kinases and phosphatases, we identified synthetic interactions with *TSC1* and *TSC2*. Individual knockdown of three candidate genes (*mRNA-cap, Pitslre and CycT;* orthologs of *RNGTT, CDK11* and *CCNT1* in humans) reduced the population growth rate of *Drosophila* cells lacking either *TSC1* or *TSC2* but not that of wild-type cells. Moreover, individual knockdown of these three genes had similar growth-inhibiting effects in mammalian TSC2-deficient cell lines, including human tumor-derived cells, illustrating the power of this cross species screening strategy to identify potential drug targets.

Introduction

The tuberous sclerosis complex (TSC) protein complex is a point of convergence of multiple upstream signaling pathways that is vital for the control of growth and proliferation in response to extracellular signals. Genetic disruption of the TSC protein complex, through mutations in *TSC1* or *TSC2*, gives rise to the TSC and lymphangioleiomyomatosis (LAM) diseases, which are systemic disorders associated with the development of widespread neoplastic lesions (*1*). Current therapeutic strategies targeting the TSC complex and the surrounding network include the Tor inhibitor rapamycin and its derivatives. However, such treatments are limited to cytostatic effects and tumors rapidly regrow following cessation of treatment (*2-4*), underscoring the need to identify new therapeutic targets for the treatment of TSC. A common limitation of chemotherapeutic agents is toxicity to healthy tissues, limiting the dose and duration of treatment and thereby restricting their efficacy. Therefore, we sought to identify potential drug targets with synthetic effects in combination with TSC complex components, in which knockdown of the target gene alone has little effect on normal cells but is toxic in TSC-deficient cells.

RNAi screens in mammalian cells have been extensively used to identify novel drug targets for various tumor types and results from these studies have led to the identification of a number of candidates. However, many candidates identified from such screens have suffered from reproducibility issues and as such few functional therapeutic targets have emerged (*5*). One way to address this issue is

to perform cross-species screens because candidates with conserved effects between organisms are more likely to be functional therapeutic targets in follow-up studies (*6*). Because the TSC signaling network is conserved between *Drosophila* and mammals and robust methods for *Drosophila* cell-based screens have been established (*6*), we decided to perform combinatorial screens in *Drosophila* cells to identify synthetic interactions with TSC1 and TSC2 (also known as Gigas) and evaluate whether the identified candidates had conserved synthetic effects in mammals.

As demonstrated in yeast studies, combinatorial screening is an effective way to identify synthetic interactions (*7, 8*). However, when multiple RNAi reagents are used in combination, the consequences of off-target effects and variable knockdown efficiencies are compounded, leading to high false-positive and false-negative rates (*9, 10*). Deconvolving biologically meaningful candidates from such screens requires extensive secondary screening and validation, making this approach time-consuming and expensive.

Here, we first describe a method for the generation of isogenic mutant *Drosophila* cell lines, which we then used for synthetic screens in *Drosophila* cells that combined CRISPR-generated cell lines deficient for TSC1 or TSC2 with RNAi screening methods. By combining these two technologies and screening in two independent TSC mutant backgrounds, we identified three robust candidate drug targets without needing to perform secondary screening. We demonstrated that

all three of these candidates have conserved synthetic interactions with TSC2 in mouse embryo fibroblasts and human tumor-derived cell lines, illustrating the power of this approach to identify potential candidates for therapeutic targeting.

Results

Optimization of the CRISPR system for *Drosophila* cell culture

CRISPR functions with high efficiency in many organisms, including *Drosophila* (*11-19*), making it an ideal system for generating mutant cell lines for combinatorial screening. However, our ability to predict off-targets and short guide RNA (sgRNA) efficacy prior to testing is currently limited and it is unclear whether design rules from mammalian systems are transferable to *Drosophila* cells (*20-23*). We therefore decided to assess the specificity of CRISPR in *Drosophila* cell culture. We first generated a vector encoding both Cas9 and sgRNA (**Supplementary file 1**) and then used this to express 75 variants of an sgRNA in S2R+ cells with different mismatches to a single target sequence present in a luciferase based reporter (**Supplementary file 2**) or in the genome. The extent and position of mismatch required to prevent mutation was assessed by measuring changes in luciferase expression from the reporter construct (**Fig. 1A**) or using high-resolution melt assays (HRMA) on endogenous sequences (**Fig. S1**). Both approaches produced similar results that are consistent with previous observations (*13, 24*). For example, in previous reports from mammalian systems (*25*), mismatches at the 5' end of the sgRNA sequences were better tolerated than at the 3' end. However, in some cases, a single mismatch was sufficient to prevent detectable mutation. In addition, we found that 3 mismatches were sufficient to prevent detectable mutations except when all mismatches were at the 5' end of the sgRNA, consistent with a previous report investigating specificity of CRISPR *in vivo* in *Drosophila* (*26*). We therefore used

3bp of mismatch as a cutoff to annotate predicted off-targets for all possible sgRNAs in the *Drosophila* genome and included these data in an updated version of our previously reported sgRNA design tool (http://www.flyrnai.org/crispr2) (*16*) (**Fig. S2**). Note that to be included in this tool, sgRNAs must have a unique 3' seed sequence. As such, no annotated sgRNA can have off-targets with mismatches clustered at the 5' end. Using these updated off-target predictions, we estimate that 97% of genes in the *Drosophila* genome can be targeted with specific sgRNAs, making this an ideal system for the generation of knockout cell lines.

Because the rate of mutations varies widely between different sgRNAs (*27-29*), we tested whether efficiency could be predicted based on the sgRNA sequence. We generated 75 additional sgRNAs each targeting luciferase-based reporter constructs with no mismatches and tested mutation efficiency for each (**Table S1**). Using this panel of sgRNAs and associated efficiencies, we first considered whether GC content correlated with mutation rate as has been suggested in several previous reports (*26, 28, 30, 31*). In contrast to the results of Ren *et al. (26)* suggesting that greater than 50% GC content in the six PAM proximal nucleotides is associated with high efficiency, we found no such correlation for any part of the sgRNA sequence (**Fig. S3A-C**). However, our observations are consistent with a mammalian study suggesting that both high and low GC content at the 3' end is associated with low efficiency (**Fig. S3B** and (*28*)) Next, we tested whether a more general sequence-based approach could improve

efficiency prediction. We analyzed the nucleotide content of all 75 sgRNAs considering each position separately and generated a probability matrix linking nucleotide content with mutation rate (**Fig. 1B**), which was used to predict efficiency scores based on sgRNA sequence. To test the performance of this approach, we generated scores for sgRNAs used in three previous *Drosophila* publications and found a strong correlation with reported efficiencies for two of them (**Fig. 1C**). Note that sgRNAs unlikely to produce a mutant phenotype (targeting close to the 3' end of genes) or with apparent viability effects (few emerging adults) were not included in this analysis. However, very little correlation was detected for a third dataset (**Fig. S3D**). In addition, the criteria that we identified for high sgRNA efficiency differ from those of two studies performed in mammalian systems (*27, 28*) and these two studies also differ from the GC requirements identified previously in *Drosophila* (*26*), suggesting that in some cases, efficiency criteria may depend on factors other than simply sgRNA sequence. Finally, we generated predicted scores for all sgRNA target sites in the *Drosophila* genome based on our findings and annotated these in our online design tool (http://www.flyrnai.org/crispr2) (**Fig. S2**). Using this updated tool, sgRNAs can be quickly designed for various applications.

Generation of stable mutant cell lines

The CRISPR system works efficiently in *Drosophila* cell culture (*11, 12*). However, it has not yet been possible to generate cell lines in which all cells are null mutants for the target gene, because previous studies have shown that

mutant populations quickly revert back to wild-type. To solve this issue, we first generated optimized sgRNAs to maximize their efficiencies while avoiding off-target effects (Figures 1 and S2). In addition, we implemented a method to predict frame-shift and in-frame mutation rate for each sgRNA target site (*32*) and annotated each of these mutation rates in our online design tool (http://www.flyrnai.org/crispr2). Second, to ensure that mutant cell lines do not revert to wild-type, a method is required to grow cultures from individual cells, a historically difficult problem with *Drosophila* cells. Various methods for this problem have been proposed (*33-35*) but none have been widely used due to either difficulty in identifying single cell-derived cultures or very low efficiencies. To substitute for paracrine factors that promote the survival of individual *Drosophila* cells cultured in populations, we tested whether the use of culture media preconditioned with wild-type S2R+ cells would allow the efficient growth of individual S2R+ cells isolated by flow cytometry. When seeded into regular media, 0 of 190 individual cells formed colonies but when seeded into conditioned media, 30 of 190 (16%) formed colonies that could be expanded into clonal cultures (**Fig. 2A**). Varying the FBS concentration had no additional effect.

One difficulty associated with the isolation of mutant cells from *Drosophila* S2R+ cells is that they are aneuploid, containing roughly 4 copies of any given genomic locus (*36*). Thus, the chances of identifying cells in which all alleles carry frame shift mutations are considerably lower than for diploid cells. To assess the ability of CRISPR to produce homozygous mutations in these cells, we targeted the

yellow gene and tested 30 individual cells for the presence of mutations using high-resolution melt (HRM) assays. 21 (70%) carried mutations at the target locus (**Fig. 2B**). The 8 samples with the strongest signal in the HRM assays were analyzed by sequencing. No wild-type sequences were detected for any of these samples, and 7/8 contained a single mutation in all derived sequences (**Fig. S4**). The identification of homozygous mutations in 7/8 cells tested is consistent with previous reports of high rates of gene conversion following genome editing (*37-39*); however, it is also possible that homozygous mutations are generated as a result of chromosome loss. Therefore, the HRM assay is an effective method to identify fully mutant clones.

Next, to test the efficacy of our sgRNA design tool and the combined CRISPR and single-cell cloning approach (**Fig. S5A**) we targeted a genes for which loss of protein function could easily be assayed: *STAT92E*, which encodes a STAT (signal transducer and activator of transcription) transcription factor that is activated by JAK (Janus kinase) (**Fig. S5B**). 15 clones were analyzed, of which 13 carried mutations on all alleles. Further testing showed that the expected phenotype was produced from these knockouts, with the STAT92E line unable to respond to JAK/STAT pathway stimulation induced by *upd* ligand overexpression (**Fig. 2C**). In addition, the effect of the *STAT92E* mutation was considerably stronger than that produced by targeting *STAT92E* with dsRNA, which reduced the response to JAK/STAT pathway stimulation but did not prevent it. These

results demonstrate that our approach provides an efficient CRISPR-based method for the production of stable, homogenous mutant *Drosophila* cell lines.

Synthetic screens using *TSC1* and *TSC2* mutant lines

We generated cell lines carrying frameshift mutations in the *TSC1* and *TSC2* genes using the approach described above (**Fig. S6**). To characterize the lines, we tested whether they showed phenotypes similar to those previously reported *in vivo* or in mammalian cell lines (*40-44*) because antibodies against *Drosophila* TSC1 or TSC2 are not available. Three phenotypes were considered: cell size, responsiveness to growth factor deprivation, and phosphorylation of the downstream Tor target S6K. *TSC1* and *TSC2* cell lines had all three phenotypes: They displayed an increased cell diameter (**Fig. 3, A to D**), an inability to modify population growth in the absence of growth factors (**Fig. 3E**), and increased phosphorylation of S6K (when normalized to α-tubulin; **Fig. 3F, G**). To further characterize the mutant cell lines, we performed phosphoproteomic analysis. 128 phosphosites showed greater than 1.5 fold increase or decrease in both mutant lines compared to wild-type cells (**Table S2**). GO analysis demonstrated that 20 of the top 30 most significantly enriched categories were consistent with known functions of the TSC network (**Fig. 3H and Table S3**), including insulin signaling, response to nutrients, and the growth of cells and tissues. Together these results suggest that the cell lines accurately represent TSC mutant models.

Next, to take advantage of the homogenous *TSC1* and *TSC2* mutant cell lines, we performed a combinatorial RNAi screen of all *Drosophila* kinases (376) and phosphatases (159). We measured population viability using a total ATP readout to capture changes in cell growth, proliferation and cell death (referred to as "population growth" from here on). Any samples with significant effects on the population growth of wild-type cells were discarded to identify TSC-specific hits. 20 of the remaining knockdowns had significant effects on *TSC1* mutant cells and 49 hits significantly affected *TSC2* mutant cells (**Fig. 4A and Table S4**). Because TSC1 and TSC2 act as part of a protein complex and mutations in either gene give rise to the TSC disease, we decided to consider for further studies genes that were identified in both the *TSC1* and *TSC2* screens. This approach filtered out the noise associated with either individual screen and identified genes with the most robust synthetic interactions with the TSC complex. The knockdown of three genes (*mRNA-cap, Pitslre* and *CycT*) showed robust and specific effects on *TSC1* and *TSC2* deficient cells (**Fig. 4A**, purple crosses).

The first candidate, mRNA-cap, is the 5' triphosphatase and guanylytransferase that catalyzes the first two steps required for the formation of a 5' 7-methylguanylate mRNA cap, which is necessary for the initiation of cap-dependent translation (*45*). Because activation of mTOR promotes cap-dependent translation initiation through multiple downstream targets (*46, 47*), our findings suggest that TSC mutant cells depended on mRNA capping, an event

that precedes the steps in translation regulated by mTOR. Our phosphoproteomic analysis identified phophosites on distinct components of the translation initiation machinery, such as Thor, eIF4G, eIF3-S10 and eIF2B, being either increased or decreased in either TSC1, TSC2 or both mutant cell lines compared to control. In addition, phosphorylation changes were detected in both cell lines for two other proteins that directly interact with core components of the translation initiation complex (Ens and Map205 – **Supplementary Table 2**) (*48, 49*).

Given the link between TSC signaling and translation initiation, we tested whether another translation initiation component showed a similar synthetic relationship with the TSC mutant cell lines. We knocked down *eIF3-S4* in wild-type, TSC1 or TSC2 mutant cells using the same assays as for the kinase and phosphatase screen. Both *TSC1* and *TSC2* mutant cells had a synthetic decrease in population growth (**Fig. 4A**, purple circle) suggesting that the control of cap-dependent translation initiation may be a promising therapeutic target for TSC dependent and/or mTORC1 hyperactive disease.

The second candidate, CycT, is a kinase implicated in the regulation of transcriptional elongation (*50, 51*). mRNA-cap is recruited to the RNA PolII C-Terminal Domain phosphorylated at Ser^5 to form the 5' mRNA Cap, and CycT promotes RNA PolII phosphorylation at this site. Thus the function of CycT may be related to that of mRNA-cap. Finally, the third candidate, Pitslre, is a cyclin

dependent kinase that has been implicated in the regulation of autophagy (*52*). Disruption of the TSC complex leads to reduced autophagy, which has been exploited previously as a potential therapeutic strategy by combining autophagy inhibitors such as Chloroquine with mTOR inhibitors (*53*).

To determine whether the identified interactions extended to *CG6182* (*TBC1D7* in mammals), a third component of the TSC complex (*54*), we tested whether combinatorial knockdown of *mRNA-cap*, *CycT* or *Pitslre* with *CG6182* (*54*) knockdown produced greater reduction in population growth than either knockdown alone. In all three cases, the combination of dsRNAs targeting the candidate gene and *CG6182* produced a synthetic reduction in population growth (**Fig. 4B**).

Conservation of synthetic interactions in mammalian cells

Because all three candidates from the *Drosophila* screens have orthologs in mammals (**Table S5**), we tested whether the synthetic interactions between *mRNA-cap, Pitslre* and *CycT* and *TSC1* and *TSC2* were conserved. We used siRNAs targeting orthologs of each of the three genes in *TSC2*-deficient MEFs compared to littermate-derived wild-type MEFs. Both *RNGTT* (*mRNA-cap* in *Drosophila*) and *CCNT1* (*CycT* in *Drosophila*) knockdowns caused reduced population growth in $TSC2^{-/-}$ cells compared to wild-type although no synthetic effect was detected with *CDK11* (*Pitslre* in *Drosophila)* because *CDK11* knockdown reduced mTORC1 activity in both the wild-type and $TSC2^{-/-}$ MEFs

(**Fig. 4C, Fig. S7A-F and Fig. S8**). We noted however that similar synthetic interactions were not detected when any of the three candidates were knocked down in combination with *TSC1*, *TSC2* or *TBC1D7* using combinatorial siRNA treatments (**Fig. S9**). These results suggest that although the target proteins were efficiently reduced (**Fig. S8**), either residual protein was sufficient to restore some function or long-term effects of loss of function of the TSC complex were required. In the latter case, although TSC proteins were depleted, the effect might not be detectable because the cells might still have enough of the components normally regulated by TSC. Further, to assess the relevance of these potential drug targets to human tumor cells, we used siRNA to knockdown the three hits in a *TSC2*-deficient human renal angiomyolipoma (AML) cell line derived from a patient with LAM (*55*). For isogenic comparison, the candidate genes were knocked down using siRNA in the same cell line stably reconstituted with wild-type TSC2. To assess the effectiveness of the TSC2 addback, we measured S6K phosphorylation and cell size with and without TSC2 reconstitution. As expected, TSC2 addback reduced mTORC1 activity and cell size (**Fig. S10**). siRNAs targeting each of the three candidate genes significantly reduced the population growth of *TSC2* null cells as assessed by using total ATP as a readout (**Fig. 4D and Fig. S7G-I**). In addition, synthetic effects were seen on cell numbers for all three genes (**Fig. 4E**). In contrast, two negative control genes that did not score in the *Drosophila* screen (*Src42A* (*FRK* in mammals) and *for* (*PRKG1* in mammals)) showed no synthetic effects (**Fig. S7J-K**),

indicating that the three gene products we have identified could be promising drug targets for TSC and LAM.

Discussion

We have developed a synthetic screening method that combines the CRISPR genome editing system with well-established RNAi methodologies. Previous combinatorial screens in *Drosophila* cells have been performed by treating cells with multiple RNAi reagents simultaneously (*9, 10*). However, whilst this approach has been used successfully, limitations of RNAi including incomplete transfection, partial knockdown and off-target effects are compounded leading to high false negative and false positive rates. Laborious and time consuming secondary screening is therefore required to identify the robust hits from these screens.

The screening strategy we have developed offers several advantages compared to combinatorial RNAi treatment. First, by combining CRISPR-generated mutant cell lines with single RNAi reagents, we avoid much of the noise associated with dual RNAi based screening approaches. The use of homogeneous populations of null mutant cells avoids the issues of incomplete transfection and incomplete knockdown. In addition, once generated, in depth characterization of the mutant cell lines can be performed to establish whether off-target mutations are present. In the case of our screen, this reduction in noise as well as the comparison between two independent mutant cell lines completely avoided the need for secondary screening.

Second, in some cases, mutant cell lines may represent a considerable improvement in the quality of disease models over RNAi mediated knockdowns. For example, diseases such as TSC are caused by loss of function mutations rather than partial transient reduction in protein abundance. The establishment of a mutant cell line enables cellular adaptation to the induced mutation, likely generating a more representative cellular environment. This is illustrated by the lack of synthetic effects detected using siRNA mediated combinatorial knockdowns in MEFs (**Fig. S9**). One implication is that future screens performed in such adapted backgrounds may lead to hits with more reproducible effects in a therapeutic setting.

Third, previous screening strategies have required laborious secondary screening and validation of hits to identify those that are robust. Here, we have simultaneously screened in two mutant backgrounds (*TSC1* and *TSC2*). Because these proteins both act as part of the TSC complex, similar effects are expected from the two knockouts. Therefore, by considering the overlap between these data sets we were able to quickly identify the most robust candidates. The advantage of this approach is reflected in the fact that the identified synthetic candidates were validated in both mammalian cell types, resulting in a very rapid translation from screening in a model organism to identification of clinically relevant potential drug targets. Finally, by considering conservation between *Drosophila* and humans, we increase the likelihood of the identified effects being reproducible, an issue that has been a major limitation in previous studies (*5*).

Current treatments for TSC related disease include rapamycin and its derivatives, which function by blocking mTor activity downstream of the TSC complex. A problem associated with this approach is that the molecular vulnerabilities caused by mutations in the TSC complex are reversed, thereby reducing the opportunities available to kill affected cells (*56*). The targets we have identified here offer the potential to bypass this issue. Indeed, none of the target genes affected the phosphorylation of S6K in AML cells when knocked down and two (CCNT1 and RNGTT) had no effect on the phosphorylation of S6K in TSC2 deficient MEFs (**Fig. S8**), suggesting that some molecular vulnerabilities caused by mTor activation may persist following inhibition of these potential drug targets. For example, inhibition of mRNA-cap would not be expected to have direct effects on autophagy, and therefore may maintain the energy stress associated with TSC mutations. However, further work will be required to determine whether inhibition of these factors is more efficacious than mTor inhibition.

Finally, whilst we have used mutant cell lines to develop an improved synthetic screening method, there are many other possible applications of stable homogeneous mutant lines. For example, modeling of diseases caused by single null mutations or epistasis experiments where residual expression of the target gene can complicate interpretation of results. We therefore expect this method to be widely applicable to many different areas of research.

In conclusion, by combining established RNAi screening methods in *Drosophila* cells with CRISPR genome-editing technology, we have developed a powerful new approach to synthetic screening. The robustness of this method is demonstrated by the conservation of the identified synthetic interactions in mouse and human systems, suggesting that it will be a generally applicable approach to investigate various biological and disease-relevant questions.

Materials and Methods

Generation of CRISPR expression vector

A *Drosophila* codon optimized *Cas9* with *3xFlag* tag and *NLS* elements at both 5' and 3' was synthesized by GenScript and the *Drosophila U6* promoter and *act5c* promoter were PCR amplified from *Drosophila* genomic DNA (**Table S6**). These were used to replace the human codon optimized *Cas9*, human *U6* and *CGh* promoters respectively of the pX330 (*13*) plasmid to yield the pl018 plasmid (**Supplementary file 1**). sgRNA homology sequences were cloned into pl018 using pairs of DNA oligonucleotides, which were annealed and ligated into *BbsI* sites according to a previously described protocol (*13*) (**Table S6**).

Luciferase-based mutation reporter assays

The luciferase reporter vector was constructed by PCR amplifying the *metallothionein* promoter from pMK33 (*59*) and *luciferase* gene from pGL3 (*60*) (**Table S6**) and combining these with annealed oligos containing a sgRNA target site (**Table S1 and Table S6**) and a custom made cloning vector using Golden Gate assembly. Luciferase assays were performed by transfecting S2R+ cells with the relevant pl018 plasmid, luciferase reporter and pRL-TK (Promega) (to allow normalization of transfection efficiencies between samples) in 96 well plates using Effectene Transfection Reagent (Qiagen) according to the manufacturer's recommendations. 24 hours after transfection, $CuSO_4$ was added to the cell media at a final concentration of 140μM and cells were incubated for a further 16 hours. Firefly and Renilla luciferase readings were taken using the

Dual-Glo Luciferase Assay System (Promega) according to manufacturer's instructions and a SpectraMax Paradigm Multi-Mode Microplate Detection Platform (Molecular Devices).

Online tools

An improved version of CRISPR design tool was implemented re-using some of the modules developed previously (*16*). Besides allowing users to choose different off-target thresholds, this version also displays pre-calculated efficiency score and restriction enzyme annotation. The efficiency score was calculated based on a probability matrix computed using the *in vitro* cell line data described in Figure 1A. It reflects cumulative p-value for high efficiency of each nucleotide from position 1 to 20 with higher values representing higher efficiency. A user interface allowing efficiency score calculation for user-provided sequences was also developed as part of the improved tool, which dynamically calculates predicted efficiency scores for each input sequence from position 1 to 20 or over a user-defined region (**Fig. S2**).

HRMAnalyzer was written as a series of Matlab programs running under control of CGI front-end implemented in Perl and Javascript. The Matlab programs are compiled as stand-alone executable programs and called from within the Perl CGI back-end script. Both tools are hosted on a shared server provided by the Research IT Group (RITG) at Harvard Medical School.

Transfections

Cells were transfected using Effectene Transfection Reagent (Qiagen) according to manufacturers instructions. For generation of mutant cell lines, we used 360ng of pl018 plasmid and 40ng actin-GFP plasmid as a marker of transfected cells. Transfections were performed in 6 well plates and unless stated otherwise, were incubated for four days at 25°C before further processing.

Production of conditioned media

S2R+ cells were incubated with fresh Schneider's media supplemented with 10% FBS for 16 hours while in log phase growth. Media was then filtered to remove cells and diluted 50% using fresh media supplemented with FBS to obtain the required final FBS concentration.

Single-cell cloning

Cloning of single cells was performed using fluorescence activated cell sorting (FACS) of GFP marked cells. Untransfected cells were used to determine background fluorescence amounts before selecting the top 10% of GFP-expressing cells for isolation. Individual cells were sorted into 96 well plates containing culture media. Following two or three weeks of culture, single cells clones were identified visually and isolated into larger cultures.

HRM assays

PCR fragments were prepared from genomic DNA as described for sequencing

analysis. Reaction products were then diluted 1:10,000 before an additional round of PCR amplification using Precision Melt Supermix (Bio-Rad) and nested primers to generate a product <120bp in length (95°C 3min, 50 rounds of [95°C 30sec, 60°C 18s, plate read], 95°C 30sec, 25°C 30sec, 10°C 30sec, 55°C 31sec, ramp from 55°C to 95°C and plate read every 0.1°C). Data was analyzed using HRMAnalyzer, available at www.flyrnai.org/HRMA. See Table S6 for primer sequences.

Sequence verification of clones

Genomic DNA was prepared from cultured cells by resuspension in 100uL of lysis buffer (10mM Tris-HCL pH8.2, 1mM EDTA, 25mM NaCl and 200ug/ml proteinase K) and incubation in a thermo cycler for 1 hour at 50°C followed by denaturation at 98°C for 10 minutes. Target sequences were cloned by PCR using Phusion high-fidelity DNA polymerase (NEB) according to manufacturer's recommendations and supplemented with an additional 2.5 mM $MgCl_2$ (35 cycles: 96°C, 30s; 50°C, 30s; 72°C, 30s). PCR products were gel purified, cloned into the pCR-Blunt II-TOPO vector (Invitrogen) and transformed into Top10 chemically competent cells (Invitrogen). Following transformation, single colonies were isolated for sequencing. To assess homozygosity of single-cell samples, a minimum of 5 colonies were sequenced per sample. For identification of mutant cell lines a minimum of 20 colonies were analyzed.

Analysis of STAT92E activity

S2R+ and *STAT92E* cell lines were transfected using Effectene Transfection Reagent (Qiagen) according to the manufacturer's instructions to introduce *upd* cDNA cloned into pMK33 expression vector, Renilla expression vector (pRL-TK, promega) and 10X-STAT-luc (*61*) into experimental samples or pMK33, pRL-TK and 10X-STAT-luc into control samples. RNAi samples included an additional 50ng of dsRNA (DRSC ID: DRSC16870 or DRSC37655) from the dsRNA template collection at the *Drosophila* RNAi Screening Center (DRSC) (www.flyrnai.org). Cells were transfected for 24 hours before addition of $CuSO_4$ at a final concentration of 140µM and incubation for a further 16 hours. Firefly and Renilla luciferase measurements were performed using a SpectraMax Paradigm Multi-Mode Microplate Detection Platform (Molecular Devices).

Cell size assays

S2R+, *TSC1* and *TSC2* mutant cell lines were analyzed using a BD Biosciences LSR Fortessa X-20 cell analyzer to measure forward scatter for each cell as a proxy for cell diameter.

Cell line growth assays

5000 cells for each line were seeded into 384 well plates containing 50µl culture media and incubated at 25°C for 5 days. 27µl of CellTiter-Glo reagent (Promega) was added to each well before reading luminescence using a SpectraMax Paradigm Multi-Mode Microplate Detection Platform (Molecular Devices).

Quantitative phosphoproteomics

Phosphoproteomic analysis was performed as described previously (*62*). Briefly, S2R+, *TSC1* or *TSC2* mutant cells were serum starved for 16 hours before lysis in 8M urea. Samples were then digested with trypsin, peptides chemically labeled with TMT Isobaric Mass Tags (Thermo Scientific), separated into 12 fractions by strong cation exchange (SCX) chromatography, purified with TiO_2 microspheres and analyzed via LC-MS/MS on an Orbitrap Velos Pro mass spectrometer (Thermo Scientific). Peptides were identified by Sequest and filtered to a 1% peptide FDR. Proteins were filtered to achieve a 2% final protein FDR (final peptide FDR near 0.15%). TMT reporter ion intensities for individual phosphopeptides were normalized to the summed reporter ion intensity for each TMT label. The localizations of phosphosites were assigned using the AScore algorithm.

Synthetic screening

S2R+, *TSC1* and *TSC2* mutant cell lines were each screened in triplicate using the 'kinases and phosphatases' sub-library provided by the DRSC (www.flyrnai.org). Screening was performed following standard procedures as described by the DRSC (www.flyrnai.org/DRSC-PRR.html). Briefly, for each 384 well plate, 5000 cells in 10ul FBS free media were seeded into each well, already containing 5ul of dsRNA at a concentration of 50ng/ul. Samples were incubated at room temperature for 45 minutes before adding 35ul of 14% FBS media (bringing final FBS concentration to 10%). Plates were incubated at 25C for five

days before assaying ATP concentrations using CellTiter-Glo assays (Promega) and a SpectraMax Paradigm Multi-Mode Microplate Detection Platform (Molecular Devices). The CellTiter-Glo Luminescent Cell Viability Assay determines the number of viable cells in culture based on quantitation of the ATP present, thus measuring changes in cell growth, proliferation and/or cell death (population growth).

CellTiter-Glo data was analyzed by normalizing data to the median value of each column (to correct for pipetting errors) and calculating z-scores for each trial individually. Z-scores greater than 1.5 or less than -1.5 in at least two out of three trials were considered to affect population growth significantly. Synthetic hits were identified as dsRNAs that significantly affect population growth of *TSC1* or *TSC2* mutant cell lines but not S2R+.

Validation of synthetic interactions in mammalian cells

TSC2$^{+/+}$*;TP53*$^{-/-}$ and *TSC2*$^{-/-}$*;TP53*$^{-/-}$ MEFs (*63*) and TSC2 deficient angiomyolipoma cells with empty vector or TSC2 addback (*64*) were transfected with siGENOME SMARTpool siRNAs (Dharmacon) targeting *CCNT1, RNGTT* or *CDK11* using Lipofectamine RNAiMAX Transfection Reagent (Invitrogen) according to manufacturers reverse transfection protocol. ATP concentrations were quantified using the CellTiter-Glo Luminescent Cell Viability Assay (Promega) according to manufacturers instructions. The following antibodies were purchased from Cell Signaling Technology and used for western blot

analysis: TSC2 #3612, phospho-T389 S6 Kinase #9234, S6 Kinase #2708, GAPDH #5174, CCNT1 #8744, CDK11 #5524. RNGTT antibody was purchased from Novus Biologicals #NBP1-49972.

Supplementary Materials

Figure S1: Analysis of CRISPR specificity using quantitative HRM

Figure S2: An improved sgRNA design tool

Figure S3: Analysis of GC content in relation to sgRNA efficiency

Figure S4: Sequencing of individual CRISPR mutant cells

Figure S5: Generation of isogenic mutant cell lines

Figure S6: Generation of *TSC1* and *TSC2* mutant cell lines

Figure S7: Synthetic effects in MEFs and AML cells

Figure S8: Analysis of knockdown of candidate genes on mTOR signaling

Figure S9: Synthetic effects of candidate genes with *TBC1D7*

Figure S10: Analysis of *TSC2* addback efficacy in AML cells

Table S1: sgRNA efficiency in relation to GC content data

Table S2: Phosphorylation changes common to *TSC1* and *TSC2* cell lines

Table S3: GO analysis of phosphoproteomic data

Table S4: Synthetic screen results

Table S5: Conservation of synthetic screen candidate genes

Table S6: Primers used in this study

Supplementary file 1: Map and GenBank sequence of CRISPR cell line expression vector (pl018)

Supplementary file 2: GenBank sequence of the luciferase mutation reporter vector

References and Notes

1. P. B. Crino, K. L. Nathanson, E. P. Henske, The tuberous sclerosis complex. *N Engl J Med* **355**, 1345-1356 (2006); published online EpubSep 28 (10.1056/NEJMra055323).

2. J. J. Bissler, F. X. McCormack, L. R. Young, J. M. Elwing, G. Chuck, J. M. Leonard, V. J. Schmithorst, T. Laor, A. S. Brody, J. Bean, S. Salisbury, D. N. Franz, Sirolimus for angiomyolipoma in tuberous sclerosis complex or lymphangioleiomyomatosis. *N Engl J Med* **358**, 140-151 (2008); published online EpubJan 10 (10.1056/NEJMoa063564).

3. F. X. McCormack, Y. Inoue, J. Moss, L. G. Singer, C. Strange, K. Nakata, A. F. Barker, J. T. Chapman, M. L. Brantly, J. M. Stocks, K. K. Brown, J. P. Lynch, 3rd, H. J. Goldberg, L. R. Young, B. W. Kinder, G. P. Downey, E. J. Sullivan, T. V. Colby, R. T. McKay, M. M. Cohen, L. Korbee, A. M. Taveira-DaSilva, H. S. Lee, J. P. Krischer, B. C. Trapnell, Efficacy and safety of sirolimus in lymphangioleiomyomatosis. *N Engl J Med* **364**, 1595-1606 (2011); published online EpubApr 28 (10.1056/NEJMoa1100391).

4. D. A. Krueger, M. M. Care, K. Holland, K. Agricola, C. Tudor, P. Mangeshkar, K. A. Wilson, A. Byars, T. Sahmoud, D. N. Franz, Everolimus for subependymal giant-cell astrocytomas in tuberous sclerosis. *N Engl J Med* **363**, 1801-1811 (2010); published online EpubNov 4 (10.1056/NEJMoa1001671).

5. W. G. Kaelin, Jr., Molecular biology. Use and abuse of RNAi to study mammalian gene function. *Science* **337**, 421-422 (2012); published online EpubJul 27 (10.1126/science.1225787).

6. S. E. Mohr, J. A. Smith, C. E. Shamu, R. A. Neumuller, N. Perrimon, RNAi screening comes of age: improved techniques and complementary approaches. *Nat Rev Mol Cell Biol* **15**, 591-600 (2014); published online EpubSep (10.1038/nrm3860).

7. A. H. Tong, M. Evangelista, A. B. Parsons, H. Xu, G. D. Bader, N. Page, M. Robinson, S. Raghibizadeh, C. W. Hogue, H. Bussey, B. Andrews, M. Tyers, C. Boone, Systematic genetic analysis with ordered arrays of yeast deletion mutants. *Science* **294**, 2364-2368 (2001); published online EpubDec 14 (10.1126/science.1065810).

8. A. H. Tong, C. Boone, Synthetic genetic array analysis in Saccharomyces cerevisiae. *Methods Mol Biol* **313**, 171-192 (2006).

9. T. Horn, T. Sandmann, B. Fischer, E. Axelsson, W. Huber, M. Boutros, Mapping of signaling networks through synthetic genetic interaction analysis by RNAi. *Nat Methods* **8**, 341-346 (2011); published online EpubApr (10.1038/nmeth.1581).

10. O. Nir, C. Bakal, N. Perrimon, B. Berger, Inference of RhoGAP/GTPase regulation using single-cell morphological data from a combinatorial RNAi screen. *Genome research* **20**, 372-380 (2010); published online EpubMar (10.1101/gr.100248.109).

11. A. R. Bassett, C. Tibbit, C. P. Ponting, J. L. Liu, Mutagenesis and homologous recombination in Drosophila cell lines using CRISPR/Cas9. *Biol Open* **3**, 42-49 (2014)10.1242/bio.20137120).

12. R. Bottcher, M. Hollmann, K. Merk, V. Nitschko, C. Obermaier, J. Philippou-Massier, I. Wieland, U. Gaul, K. Forstemann, Efficient chromosomal gene modification with CRISPR/cas9 and PCR-based homologous recombination donors in cultured Drosophila cells. *Nucleic Acids Res* **42**, e89 (2014)10.1093/nar/gku289).

13. L. Cong, F. A. Ran, D. Cox, S. Lin, R. Barretto, N. Habib, P. D. Hsu, X. Wu, W. Jiang, L. A. Marraffini, F. Zhang, Multiplex genome engineering using CRISPR/Cas systems. *Science* **339**, 819-823 (2013); published online EpubFeb 15 (10.1126/science.1231143).

14. S. J. Gratz, A. M. Cummings, J. N. Nguyen, D. C. Hamm, L. K. Donohue, M. M. Harrison, J. Wildonger, K. M. O'Connor-Giles, Genome engineering of Drosophila with the CRISPR RNA-guided Cas9 nuclease. *Genetics*

194, 1029-1035 (2013); published online EpubAug (10.1534/genetics.113.152710).

15. P. Mali, L. Yang, K. M. Esvelt, J. Aach, M. Guell, J. E. DiCarlo, J. E. Norville, G. M. Church, RNA-guided human genome engineering via Cas9. *Science* **339**, 823-826 (2013); published online EpubFeb 15 (10.1126/science.1232033).

16. X. Ren, J. Sun, B. E. Housden, Y. Hu, C. Roesel, S. Lin, L. P. Liu, Z. Yang, D. Mao, L. Sun, Q. Wu, J. Y. Ji, J. Xi, S. E. Mohr, J. Xu, N. Perrimon, J. Q. Ni, Optimized gene editing technology for Drosophila melanogaster using germ line-specific Cas9. *Proc Natl Acad Sci U S A* **110**, 19012-19017 (2013); published online EpubNov 19 (10.1073/pnas.1318481110).

17. A. R. Bassett, C. Tibbit, C. P. Ponting, J. L. Liu, Highly efficient targeted mutagenesis of Drosophila with the CRISPR/Cas9 system. *Cell Rep* **4**, 220-228 (2013); published online EpubJul 11 (10.1016/j.celrep.2013.06.020).

18. Z. L. Sebo, H. B. Lee, Y. Peng, Y. Guo, A simplified and efficient germline-specific CRISPR/Cas9 system for Drosophila genomic engineering. *Fly (Austin)* **8**, 52-57 (2014); published online EpubJan-Mar (10.4161/fly.26828).

19. Z. Yu, M. Ren, Z. Wang, B. Zhang, Y. S. Rong, R. Jiao, G. Gao, Highly efficient genome modifications mediated by CRISPR/Cas9 in Drosophila. *Genetics* **195**, 289-291 (2013); published online EpubSep (10.1534/genetics.113.153825).

20. Y. Fu, J. A. Foden, C. Khayter, M. L. Maeder, D. Reyon, J. K. Joung, J. D. Sander, High-frequency off-target mutagenesis induced by CRISPR-Cas nucleases in human cells. *Nat Biotechnol* **31**, 822-826 (2013); published online EpubSep (10.1038/nbt.2623).

21. P. D. Hsu, D. A. Scott, J. A. Weinstein, F. A. Ran, S. Konermann, V. Agarwala, Y. Li, E. J. Fine, X. Wu, O. Shalem, T. J. Cradick, L. A. Marraffini, G. Bao, F. Zhang, DNA targeting specificity of RNA-guided Cas9 nucleases. *Nat Biotechnol* **31**, 827-832 (2013); published online EpubSep (10.1038/nbt.2647).

22. P. Mali, J. Aach, P. B. Stranges, K. M. Esvelt, M. Moosburner, S. Kosuri, L. Yang, G. M. Church, CAS9 transcriptional activators for target specificity screening and paired nickases for cooperative genome engineering. *Nat Biotechnol* **31**, 833-838 (2013); published online EpubSep (10.1038/nbt.2675).

23. V. Pattanayak, S. Lin, J. P. Guilinger, E. Ma, J. A. Doudna, D. R. Liu, High-throughput profiling of off-target DNA cleavage reveals RNA-

programmed Cas9 nuclease specificity. *Nat Biotechnol* **31**, 839-843 (2013); published online EpubSep (10.1038/nbt.2673).

24. M. Jinek, K. Chylinski, I. Fonfara, M. Hauer, J. A. Doudna, E. Charpentier, A programmable dual-RNA-guided DNA endonuclease in adaptive bacterial immunity. *Science* **337**, 816-821 (2012); published online EpubAug 17 (10.1126/science.1225829).

25. P. D. Hsu, D. A. Scott, J. A. Weinstein, F. A. Ran, S. Konermann, V. Agarwala, Y. Li, E. J. Fine, X. Wu, O. Shalem, T. J. Cradick, L. A. Marraffini, G. Bao, F. Zhang, DNA targeting specificity of RNA-guided Cas9 nucleases. *Nat Biotechnol* **31**, 827-832 (2013); published online EpubSep (10.1038/nbt.2647).

26. X. Ren, Z. Yang, J. Xu, J. Sun, D. Mao, Y. Hu, S. J. Yang, H. H. Qiao, X. Wang, Q. Hu, P. Deng, L. P. Liu, J. Y. Ji, J. B. Li, J. Q. Ni, Enhanced specificity and efficiency of the CRISPR/Cas9 system with optimized sgRNA parameters in Drosophila. *Cell Rep* **9**, 1151-1162 (2014); published online EpubNov 6 (10.1016/j.celrep.2014.09.044).

27. J. G. Doench, E. Hartenian, D. B. Graham, Z. Tothova, M. Hegde, I. Smith, M. Sullender, B. L. Ebert, R. J. Xavier, D. E. Root, Rational design of highly active sgRNAs for CRISPR-Cas9-mediated gene inactivation. *Nat Biotechnol*, (2014); published online EpubSep 3 (10.1038/nbt.3026).

28. T. Wang, J. J. Wei, D. M. Sabatini, E. S. Lander, Genetic screens in human cells using the CRISPR-Cas9 system. *Science* **343**, 80-84 (2014); published online EpubJan 3 (10.1126/science.1246981).

29. O. Shalem, N. E. Sanjana, E. Hartenian, X. Shi, D. A. Scott, T. S. Mikkelsen, D. Heckl, B. L. Ebert, D. E. Root, J. G. Doench, F. Zhang, Genome-scale CRISPR-Cas9 knockout screening in human cells. *Science* **343**, 84-87 (2014); published online EpubJan 3 (10.1126/science.1247005).

30. W. Fujii, K. Kawasaki, K. Sugiura, K. Naito, Efficient generation of large-scale genome-modified mice using gRNA and CAS9 endonuclease. *Nucleic Acids Res* **41**, e187 (2013); published online EpubNov 1 (10.1093/nar/gkt772).

31. L. E. Jao, S. R. Wente, W. Chen, Efficient multiplex biallelic zebrafish genome editing using a CRISPR nuclease system. *Proc Natl Acad Sci U S A* **110**, 13904-13909 (2013); published online EpubAug 20 (10.1073/pnas.1308335110).

32. S. Bae, J. Kweon, H. S. Kim, J. S. Kim, Microhomology-based choice of Cas9 nuclease target sites. *Nat Methods* **11**, 705-706 (2014); published online EpubJul (10.1038/nmeth.3015).

33. R. A. Lindquist, K. A. Ottina, D. B. Wheeler, P. P. Hsu, C. C. Thoreen, D. A. Guertin, S. M. Ali, S. Sengupta, Y. D. Shaul, M. R. Lamprecht, K. L. Madden, A. R. Papallo, T. R. Jones, D. M. Sabatini, A. E. Carpenter, Genome-scale RNAi on living-cell microarrays identifies novel regulators of Drosophila melanogaster TORC1-S6K pathway signaling. *Genome research* **21**, 433-446 (2011); published online EpubMar (10.1101/gr.111492.110).

34. R. A. Neumuller, F. Wirtz-Peitz, S. Lee, Y. Kwon, M. Buckner, R. A. Hoskins, K. J. Venken, H. J. Bellen, S. E. Mohr, N. Perrimon, Stringent analysis of gene function and protein-protein interactions using fluorescently tagged genes. *Genetics* **190**, 931-940 (2012); published online EpubMar (10.1534/genetics.111.136465).

35. L. Cherbas, R. Moss, P. Cherbas, Transformation techniques for Drosophila cell lines. *Methods Cell Biol* **44**, 161-179 (1994).

36. H. Lee, C. McManus, D. Y. Cho, M. Eaton, F. Renda, M. Somma, L. Cherbas, G. May, S. Powell, D. Zhang, L. Zhan, A. Resch, J. Andrews, S. E. Celniker, P. Cherbas, T. M. Przytycka, M. Gatti, B. Oliver, B. Graveley, D. MacAlpine, DNA copy number evolution in Drosophila cell lines. *Genome Biol* **15**, R70 (2014); published online EpubAug 28 (10.1186/gb-2014-15-8-r70).

37. D. F. Carlson, W. Tan, S. G. Lillico, D. Stverakova, C. Proudfoot, M. Christian, D. F. Voytas, C. R. Long, C. B. Whitelaw, S. C. Fahrenkrug, Efficient TALEN-mediated gene knockout in livestock. *Proc Natl Acad Sci U S A* **109**, 17382-17387 (2012); published online EpubOct 23 (10.1073/pnas.1211446109).

38. G. F. Richard, D. Viterbo, V. Khanna, V. Mosbach, L. Castelain, B. Dujon, Highly specific contractions of a single CAG/CTG trinucleotide repeat by TALEN in yeast. *PLoS One* **9**, e95611 (2014)10.1371/journal.pone.0095611).

39. K. Li, G. Wang, T. Andersen, P. Zhou, W. T. Pu, Optimization of genome engineering approaches with the CRISPR/Cas9 system. *PLoS One* **9**, e105779 (2014)10.1371/journal.pone.0105779).

40. T. Nobukini, G. Thomas, The mTOR/S6K signalling pathway: the role of the TSC1/2 tumour suppressor complex and the proto-oncogene Rheb. *Novartis Found Symp* **262**, 148-154; discussion 154-149, 265-148 (2004).

41. J. Huang, B. D. Manning, The TSC1-TSC2 complex: a molecular switchboard controlling cell growth. *Biochem J* **412**, 179-190 (2008); published online EpubJun 1 (10.1042/BJ20080281).

42. D. A. Guertin, K. V. Guntur, G. W. Bell, C. C. Thoreen, D. M. Sabatini, Functional genomics identifies TOR-regulated genes that control growth and division. *Curr Biol* **16**, 958-970 (2006); published online EpubMay 23 (10.1016/j.cub.2006.03.084).

43. D. J. Kwiatkowski, B. D. Manning, Tuberous sclerosis: a GAP at the crossroads of multiple signaling pathways. *Hum Mol Genet* **14 Spec No. 2**, R251-258 (2005); published online EpubOct 15 (10.1093/hmg/ddi260).

44. N. Tapon, N. Ito, B. J. Dickson, J. E. Treisman, I. K. Hariharan, The Drosophila tuberous sclerosis complex gene homologs restrict cell growth and cell proliferation. *Cell* **105**, 345-355 (2001); published online EpubMay 4 (

45. S. Dunn, V. H. Cowling, Myc and mRNA capping. *Biochim Biophys Acta* **1849**, 501-505 (2015); published online EpubMay (10.1016/j.bbagrm.2014.03.007).

46. C. G. Proud, Regulation of protein synthesis by insulin. *Biochem Soc Trans* **34**, 213-216 (2006); published online EpubApr (10.1042/BST20060213).

47. M. K. Holz, B. A. Ballif, S. P. Gygi, J. Blenis, mTOR and S6K1 mediate assembly of the translation preinitiation complex through dynamic protein

interchange and ordered phosphorylation events. *Cell* **123**, 569-580 (2005); published online EpubNov 18 (10.1016/j.cell.2005.10.024).

48. K. G. Guruharsha, J. F. Rual, B. Zhai, J. Mintseris, P. Vaidya, N. Vaidya, C. Beekman, C. Wong, D. Y. Rhee, O. Cenaj, E. McKillip, S. Shah, M. Stapleton, K. H. Wan, C. Yu, B. Parsa, J. W. Carlson, X. Chen, B. Kapadia, K. VijayRaghavan, S. P. Gygi, S. E. Celniker, R. A. Obar, S. Artavanis-Tsakonas, A protein complex network of Drosophila melanogaster. *Cell* **147**, 690-703 (2011); published online EpubOct 28 (10.1016/j.cell.2011.08.047).

49. S. Lee, M. Nahm, M. Lee, M. Kwon, E. Kim, A. D. Zadeh, H. Cao, H. J. Kim, Z. H. Lee, S. B. Oh, J. Yim, P. A. Kolodziej, S. Lee, The F-actin-microtubule crosslinker Shot is a platform for Krasavietz-mediated translational regulation of midline axon repulsion. *Development* **134**, 1767-1777 (2007); published online EpubMay (10.1242/dev.02842).

50. A. A. Kiger, B. Baum, S. Jones, M. R. Jones, A. Coulson, C. Echeverri, N. Perrimon, A functional genomic analysis of cell morphology using RNA interference. *Journal of biology* **2**, 27 (2003)10.1186/1475-4924-2-27).

51. J. T. Lis, P. Mason, J. Peng, D. H. Price, J. Werner, P-TEFb kinase recruitment and function at heat shock loci. *Genes & development* **14**, 792-803 (2000); published online EpubApr 1 (

52. S. Wilkinson, D. R. Croft, J. O'Prey, A. Meedendorp, M. O'Prey, C. Dufes, K. M. Ryan, The cyclin-dependent kinase PITSLRE/CDK11 is required for successful autophagy. *Autophagy* **7**, 1295-1301 (2011); published online EpubNov (10.4161/auto.7.11.16646).

53. A. A. Parkhitko, C. Priolo, J. L. Coloff, J. Yun, J. J. Wu, K. Mizumura, W. Xu, I. A. Malinowska, J. Yu, D. J. Kwiatkowski, J. W. Locasale, J. M. Asara, A. M. Choi, T. Finkel, E. P. Henske, Autophagy-dependent metabolic reprogramming sensitizes TSC2-deficient cells to the antimetabolite 6-aminonicotinamide. *Mol Cancer Res* **12**, 48-57 (2014); published online EpubJan (10.1158/1541-7786.MCR-13-0258-T).

54. C. C. Dibble, W. Elis, S. Menon, W. Qin, J. Klekota, J. M. Asara, P. M. Finan, D. J. Kwiatkowski, L. O. Murphy, B. D. Manning, TBC1D7 is a third subunit of the TSC1-TSC2 complex upstream of mTORC1. *Mol Cell* **47**, 535-546 (2012); published online EpubAug 24 (10.1016/j.molcel.2012.06.009).

55. P. S. Lee, S. W. Tsang, M. A. Moses, Z. Trayes-Gibson, L. L. Hsiao, R. Jensen, R. Squillace, D. J. Kwiatkowski, Rapamycin-insensitive up-regulation of MMP2 and other genes in tuberous sclerosis complex 2-deficient lymphangioleiomyomatosis-like cells. *American journal of respiratory cell and molecular biology* **42**, 227-234 (2010); published online EpubFeb (10.1165/rcmb.2009-0050OC).

56. D. Medvetz, C. Priolo, E. P. Henske, Therapeutic targeting of cellular metabolism in cells with hyperactive mTORC1: A paradigm shift. *Mol Cancer Res*, (2014); published online EpubOct 8 (10.1158/1541-7786.MCR-14-0343).

57. K. J. Beumer, J. K. Trautman, A. Bozas, J. L. Liu, J. Rutter, J. G. Gall, D. Carroll, Efficient gene targeting in Drosophila by direct embryo injection with zinc-finger nucleases. *Proc Natl Acad Sci U S A* **105**, 19821-19826 (2008); published online EpubDec 16 (10.1073/pnas.0810475105).

58. N. Grecz, T. L. Hammer, C. J. Robnett, M. D. Long, Freeze-thaw injury: evidence for double strand breaks in Escherichia coli DNA. *Biochem Biophys Res Commun* **93**, 1110-1113 (1980); published online EpubApr 29 (

59. M. R. Koelle, W. S. Talbot, W. A. Segraves, M. T. Bender, P. Cherbas, D. S. Hogness, The Drosophila EcR gene encodes an ecdysone receptor, a new member of the steroid receptor superfamily. *Cell* **67**, 59-77 (1991); published online EpubOct 4 (

60. A. Krejci, F. Bernard, B. E. Housden, S. Collins, S. J. Bray, Direct response to Notch activation: signaling crosstalk and incoherent logic. *Sci Signal* **2**, ra1 (2009)10.1126/scisignal.2000140).

61. E. A. Bach, L. A. Ekas, A. Ayala-Camargo, M. S. Flaherty, H. Lee, N. Perrimon, G. H. Baeg, GFP reporters detect the activation of the Drosophila JAK/STAT pathway in vivo. *Gene expression patterns : GEP* **7**, 323-331 (2007); published online EpubJan (10.1016/j.modgep.2006.08.003).

62. R. Sopko, M. Foos, A. Vinayagam, B. Zhai, R. Binari, Y. Hu, S. Randklev, L. A. Perkins, S. P. Gygi, N. Perrimon, Combining genetic perturbations and proteomics to examine kinase-phosphatase networks in Drosophila embryos. *Developmental cell* **31**, 114-127 (2014); published online EpubOct 13 (10.1016/j.devcel.2014.07.027).

63. H. Zhang, G. Cicchetti, H. Onda, H. B. Koon, K. Asrican, N. Bajraszewski, F. Vazquez, C. L. Carpenter, D. J. Kwiatkowski, Loss of Tsc1/Tsc2 activates mTOR and disrupts PI3K-Akt signaling through downregulation of PDGFR. *The Journal of clinical investigation* **112**, 1223-1233 (2003); published online EpubOct (10.1172/JCI17222).

64. C. Li, P. S. Lee, Y. Sun, X. Gu, E. Zhang, Y. Guo, C. L. Wu, N. Auricchio, C. Priolo, J. Li, A. Csibi, A. Parkhitko, T. Morrison, A. Planaguma, S. Kazani, E. Israel, K. F. Xu, E. P. Henske, J. Blenis, B. D. Levy, D. Kwiatkowski, J. J. Yu, Estradiol and mTORC2 cooperate to enhance prostaglandin biosynthesis and tumorigenesis in TSC2-deficient LAM

cells. *The Journal of experimental medicine* **211**, 15-28 (2014); published online EpubJan 13 (10.1084/jem.20131080).

65. J. A. Vizcaino, E. W. Deutsch, R. Wang, A. Csordas, F. Reisinger, D. Rios, J. A. Dianes, Z. Sun, T. Farrah, N. Bandeira, P. A. Binz, I. Xenarios, M. Eisenacher, G. Mayer, L. Gatto, A. Campos, R. J. Chalkley, H. J. Kraus, J. P. Albar, S. Martinez-Bartolome, R. Apweiler, G. S. Omenn, L. Martens, A. R. Jones, H. Hermjakob, ProteomeXchange provides globally coordinated proteomics data submission and dissemination. *Nat Biotechnol* **32**, 223-226 (2014); published online EpubMar (10.1038/nbt.2839).

Acknowledgments: We thank David Sabatini for useful discussion on cell cloning, David Doupé for useful discussion on homologous recombination, Ian Flockhart for help with the development of HRMA data analysis tools, and Elizabeth Henske for the AML-derived cell line. **Funding:** This work was supported by NIH (5R01DK088718, 5P01CA120964 and R01GM067761) and DOD (W81XWH-12-1-0179). S.E.M. also receives support from the Dana Farber/Harvard Cancer Center, which is supported in part by NCI Cancer Center Support Grant # NIH 5 P30 CA06516. N.P. is a Howard Hughes Medical Institute investigator. R.S. is a Special Fellow of the Leukemia and Lymphoma Society.
Author contributions: BEH, SM, BDM and NP designed experiments, BEH, AJV, CK, RS, SL, MB and RT performed experiments, BEH, YH and CR developed the online CRISPR design tools, BEH, RS and YH analyzed experimental results and BEH and NP wrote the paper. **Competing interests:** BEH, AJV, BDM and NP have filed a provisional patent regarding the targeting of CCNT1, RNGTT, and CDK11 in Tuberous Sclerosis Complex. The other authors declare that they have no competing interests. **Data availability:** The mass spectrometry phosphoproteomics data have been deposited to the ProteomeXchange Consortium (*65*) via the PRIDE partner repository with the dataset identifier PXD002670.

Figure legends

Figure 1: Optimization of the CRISPR system for *Drosophila* cell culture

A: Graph showing relative mutation rates from 75 sgRNAs used to target a single sequence cloned into a luciferase reporter. Mutation rate is calculated as 1/Firefly luciferase activity normalized to Renilla luciferase activity to control for differential transfection efficiency. Bars show mean relative mutation rates from three biological replicates using sgRNAs with 0 mismatches (blue bar), 1 mismatch (grey bars), 2 mismatches (green bars), ≥3 mismatches (black bars) or in the absence of sgRNA (red bar). Dashes indicate nucleotides that are matched between sgRNA and the target sequence. Crosses indicate the position of mismatches. **B:** Matrix showing enrichment p-values of each nucleotide in each position amongst high efficiency sgRNAs. **C:** Validation of efficiency scores generated using the matrix in (B) by correlating score (horizontal axis) with efficiency (vertical axis) from two independent publications (see Figure S3D for comparison with an additional dataset).

Figure 2: Generation of mutant cell lines

A: Survival rates of single S2R+ cells seeded into different media formulations. 'Clones' represents the number of seeded samples that produced viable populations of cells three weeks after seeding. Schneider's media was supplemented with FBS at the concentrations indicated and was preconditioned using S2R+ cells where indicated. **B:** HRMA results for single S2R+ cells from a

population four days after treatment with CRISPR targeting the *yellow* gene. The graph shows the difference in fluorescence between each sample and a mean control curve against temperature (scale from 76°C to 84°C). **C:** Graph showing relative Firefly luciferase activity normalized to Renilla luciferase activity for either wild-type (black bars) or *STAT92E* (grey bars) mutant cells in the presence or absence of JAK/STAT pathway activation (*upd* ligand overexpression) and with or without activation in the presence of two different dsRNAs targeting *STAT92E* (RNAi-1 and RNAi-2). Bars show the mean from five biological replicates and error bars represent standard error of the mean. All differences between wild-type and STAT92E cells were significant ($p<0.05$).

Figure 3: Characterization of TSC mutant cell lines

A-C: Images of representative fields from wild-type (A), *TSC1* mutant (B) or *TSC2* mutant (C) cell lines. All images were taken at the same magnification and using the same settings. Scale bar represents 50µm. **D:** Graph showing frequency of cell sizes for the cell lines indicated, divided into 'low diameter' (grey bars) or 'high diameter' (black bars) using a cutoff at which the majority of wild-type cells fall into the 'low diameter' category. Bars represent the mean from three biological replicates and error bars indicate standard error of the mean. **E:** Graph showing relative rates of population growth for the cell lines indicated in either complete media (10% FBS – blue bars), under partial serum starvation conditions (1% FBS – red bars) or complete serum starvation conditions (0% FBS – green bars). Note that these values represent a combination of cell growth

and proliferation. Bars show the mean of 24 samples per cell line and condition and error bars represent standard error of the mean. **F:** Images of Western Blots stained for p-S6K or Tubulin-alpha as indicated. Samples represent biological triplicates from S2R+, TSC1 and TSC2 cells. p-S6K levels were normalized to Tubulin-alpha because an antibody for *Drosophila* total S6K was not available. **G:** Quantification of phosphorylated S6K (p-S6K) for the cell lines indicated as shown in the Western Blots in Figure 3E. Bars represent mean fold change in p-S6K normalized to Tubulin-alpha for three biological replicates in each case. Error bars represent standard error of the mean and asterisks indicate significant differences from control ($p \leq 0.01$) based on t-tests. **H:** Graph indicating the fold enrichment of the indicated GO categories in phosphoproteomic data from *TSC1* and *TSC2* mutant cells compared to wild-type. All samples are enriched with p-values less than 0.05.

Figure 4: Identification of TSC specific drug targets using synthetic screening

A: Scatter plot showing results of screens in *Drosophila TSC1* and *TSC2* mutant cell lines. dsRNAs that showed changes (see Materials and Methods) in wild-type cells are not shown on the graph. Points indicate the Z-score from three replicate screens in *TSC1* cells (horizontal axis) and *TSC2* cells (vertical axis). Dots represent candidates with no significant effect (black circles), *TSC1* specific candidates (red circles), *TSC2* specific candidates (blue circles) and candidates from *TSC1* and *TSC2* cells (purple crosses). The three genes showing synthetic reductions in population growth with both *TSC1* and *TSC2* are labeled. In addition, results for *eIF3-S4* are plotted on the same graph for comparison (purple circle). **B:** Graph showing relative viability (measured using CellTiter-Glo) for S2R+ cells treated with control (*lacZ*) dsRNA (blue bars), or two different dsRNAs targeting *CG6182* (red and green bars) in combination with dsRNAs targeting *CycT*, *Pitslre*, *mRNA-cap* or *lacZ*. Bars represent mean values from three biological replicates normalized to control dsRNA treatments. Error bars indicate standard error of the mean. **C:** Summary plots showing one time point from population growth assays in TSC2 deficient or wild-type MEFs treated with the siRNAs indicated (see Figure S7 for full time courses). Boxplots represent median (thick black lines), interquartile range (boxes) and min/max (error bars) from two biological replicates for the genes indicated in TSC2 deficient or wild-type backgrounds. The vertical axis represents change in ATP concentrations after 48 hours of culture relative to cells treated with control siRNA measured

using CellTiter-Glo assays. **D:** Summary plots showing one time point from population growth assays in TSC2 deficient AML cells. Boxplots are as described in C and represent three biological replicates (see Figure S7 for full time courses). All differences between TSC deficient and wild-type cells are significant ($p<0.05$). **E:** Graph showing relative cell numbers following siRNA-mediated knockdown of the genes indicated in AML cells with (black bars) or without (grey bars) TSC2 addback. Bars represent the average of at least four biological replicates and error bars indicate standard error of the mean. Differences between TSC2 addback and Empty vector conditions were significant for all three genes tested ($p<0.05$).

A

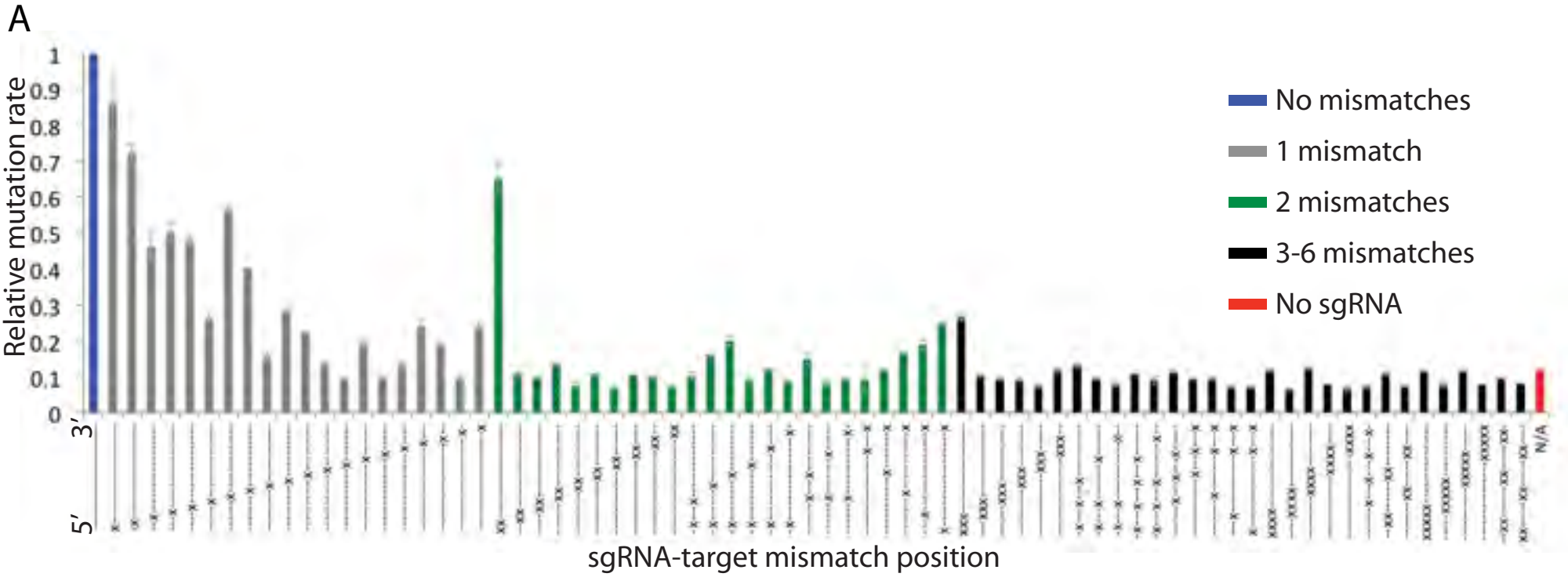

B

	1	2	3	4	5	6	7	8	9	10
A	0.4979	0.7959	0.7553	0.6569	**0.9481**	0.7147	0.4370	0.6212	**0.9077**	**1.0000**
T	0.6699	0.5485	0.2750	0.5972	0.6212	0.7555	**1.0000**	0.5131	**0.8608**	0.7553
C	0.4979	0.6869	0.8528	0.7643	0.5325	0.3417	0.3417	0.7643	0.6434	**0.0092**
G	0.7918	0.4461	0.4851	0.4461	0.3417	0.6869	0.2417	0.5485	**0.0947**	**0.9256**

	11	12	13	14	15	16	17	18	19	20
A	**0.1957**	0.7959	0.6212	0.8912	**1.0000**	0.5485	**0.9942**	0.5485	0.4550	**1.0000**
T	0.6569	0.3417	**1.0000**	**0.0160**	**0.9146**	0.7555	0.2906	0.4979	0.5485	0.5131
C	**0.9331**	0.5325	0.7272	0.9708	0.2905	0.7272	0.2957	0.7918	0.6434	0.5062
G	0.5325	0.8308	**0.1255**	0.7918	0.2544	0.4461	0.4979	0.6212	0.7918	0.4461

C

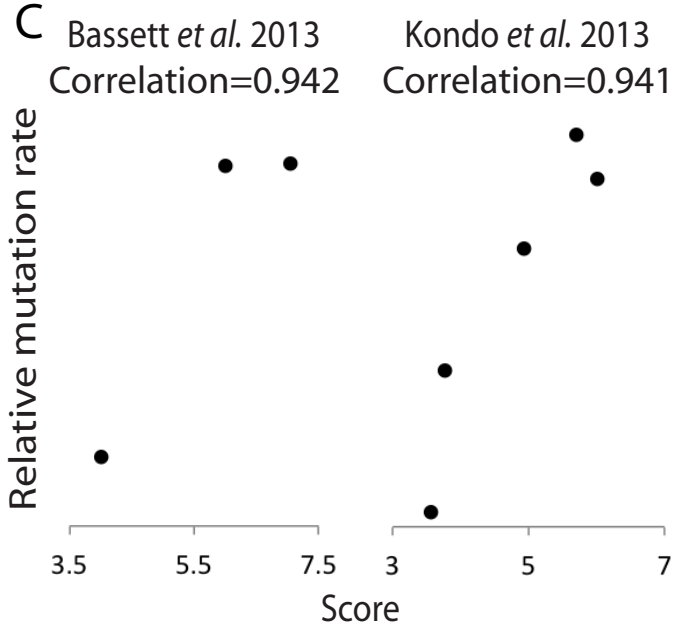

A

Media		Clones	% survival
Schneider's	10% FBS	0	0.0
	15% FBS	0	0.0
	20% FBS	0	0.0
Conditioned Schneider's	10% FBS	30	15.8
	15% FBS	31	16.3
	20% FBS	32	16.8

B

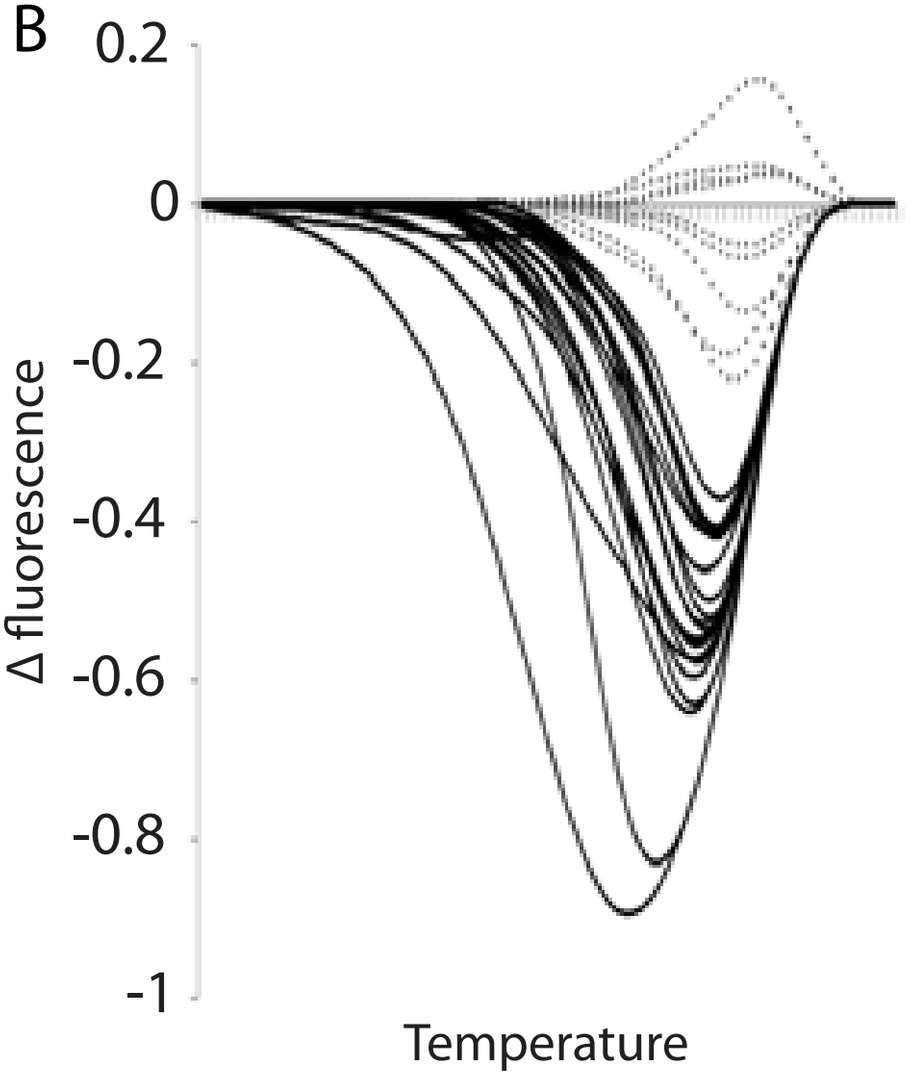

C

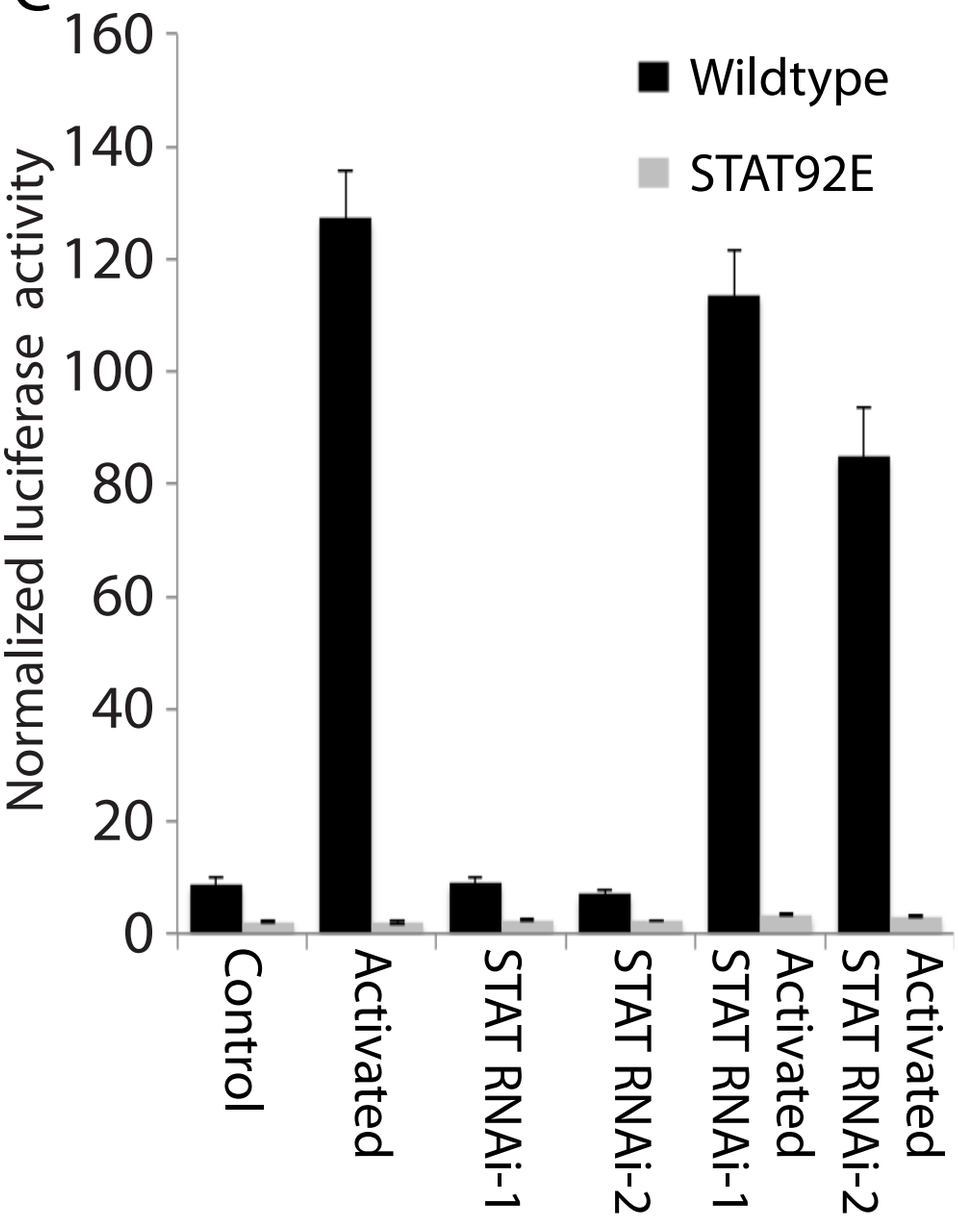

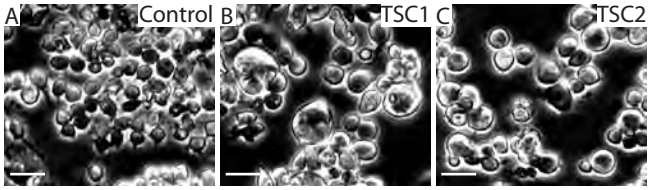
A
Control
B
TSC1
C
TSC2

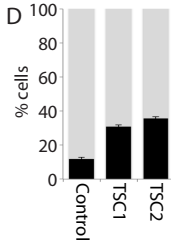
D
% cells
100
80
60
40
20
0
Control
TSC1
TSC2

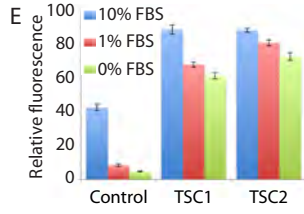
E
Relative fluorescence
100
80
60
40
20
0
10% FBS
1% FBS
0% FBS
Control
TSC1
TSC2

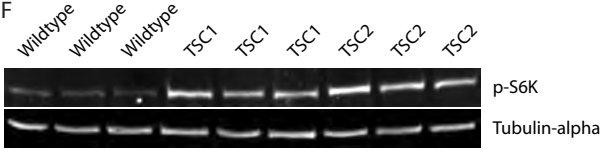
F
Wildtype
Wildtype
Wildtype
TSC1
TSC1
TSC1
TSC2
TSC2
TSC2
p-S6K
Tubulin-alpha

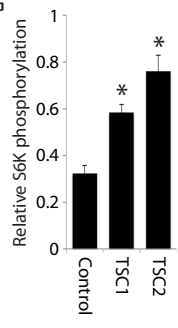
G
Relative S6K phosphorylation
1
0.8
0.6
0.4
0.2
0
*
*
Control
TSC1
TSC2

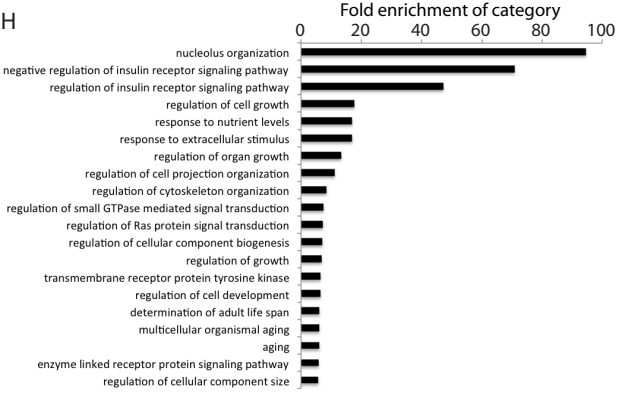
H
Fold enrichment of category
0
20
40
60
80
100
nucleolus organization
negative regulation of insulin receptor signaling pathway
regulation of insulin receptor signaling pathway
regulation of cell growth
response to nutrient levels
response to extracellular stimulus
regulation of organ growth
regulation of cell projection organization
regulation of cytoskeleton organization
regulation of small GTPase mediated signal transduction
regulation of Ras protein signal transduction
regulation of cellular component biogenesis
regulation of growth
transmembrane receptor protein tyrosine kinase
regulation of cell development
determination of adult life span
multicellular organismal aging
aging
enzyme linked receptor protein signaling pathway
regulation of cellular component size

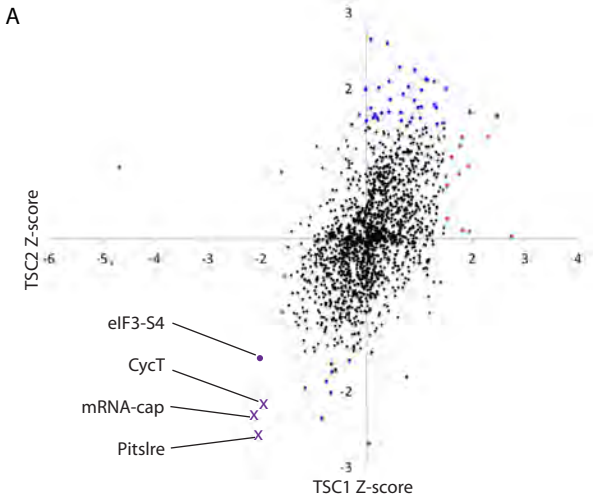
A
TSC2 Z-score
TSC1 Z-score
eIF3-S4
CycT
mRNA-cap
PitsIre

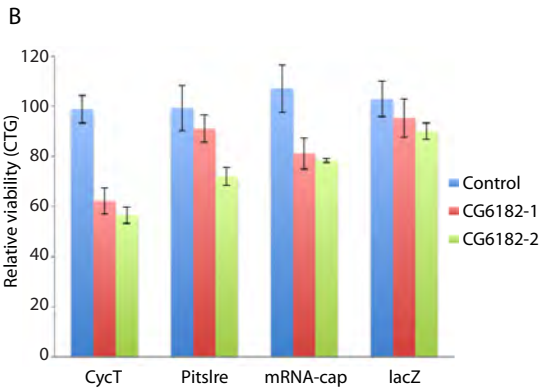
B
Relative viability (CTG)
Control
CG6182-1
CG6182-2
CycT
PitsIre
mRNA-cap
lacZ

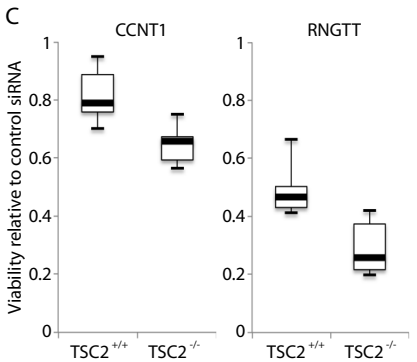
C
CCNT1
RNGTT
Viability relative to control siRNA
TSC2 +/+
TSC2 -/-

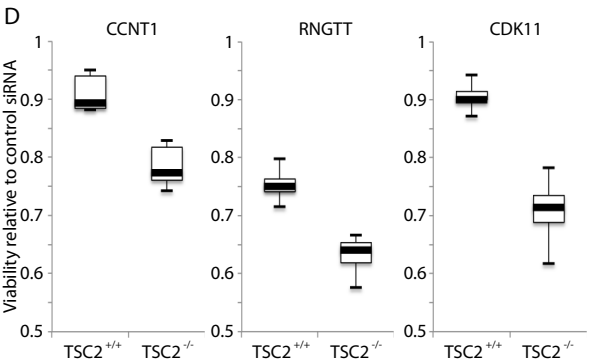
D
CCNT1
RNGTT
CDK11
Viability relative to control siRNA
TSC2 +/+
TSC2 -/-

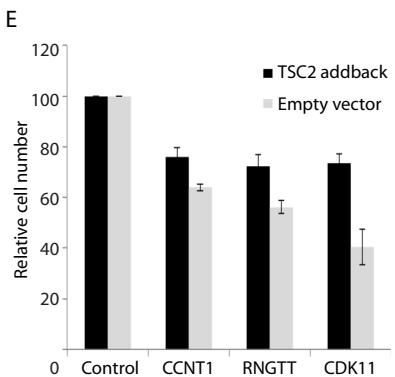
E
TSC2 addback
Empty vector
Relative cell number
Control
CCNT1
RNGTT
CDK11

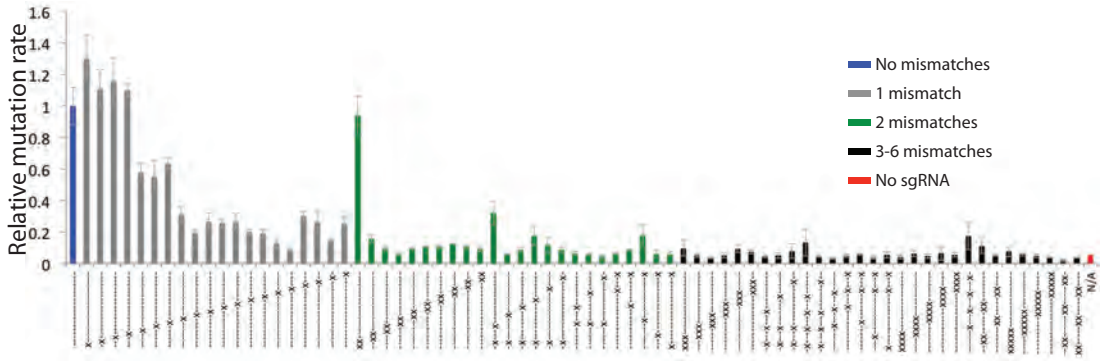

Figure S1: Analysis of CRISPR specificity using quantitative HRM

Graph showing relative mutation rates from 75 sgRNAs used to target a single sequence in the *yellow* gene. Mutation rate is calculated as integrated area between each experimental HRM curve and a mean control curve. Each bar represents the mean relative mutation rate from three biological replicates using sgRNAs with 0 mismatches (blue bar), 1 mismatch (grey bars), 2 mismatches (green bars), ≥3 mismatches (black bars) or in the absence of sgRNA (red bar). Dashes indicate nucleotides that are matched between sgRNA and the target sequence. Crosses indicate the position of mismatches. Error bars indicate standard error of the mean.

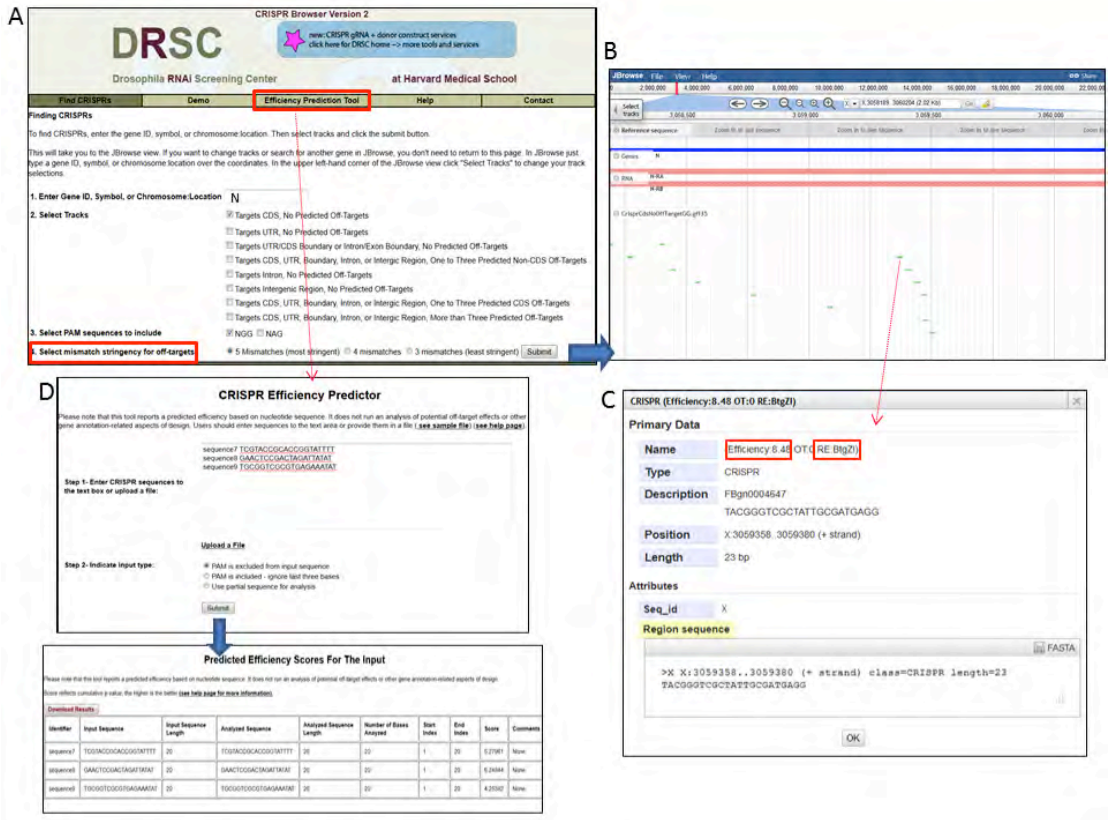

Figure S2: An improved sgRNA design tool

A: Main search page, allowing the user to search by gene symbol, CG number, FBgn as well as genome coordinates. The user also has the option of choosing the off-target threshold as well as the relevant track(s), which are divided based on whether off-targets are predicted and the genomic location of the sgRNA. **B:** JBrowse view of all relevant CRISPR designs. **C:** Detailed information page of each sgRNA design. Efficiency score predictions as well as restriction enzyme annotations are displayed beside the target gene, sgRNA sequence and genome location. **D:** Efficiency prediction tool. This user interface allows calculation of efficiency scores for user-provided sgRNA sequences.

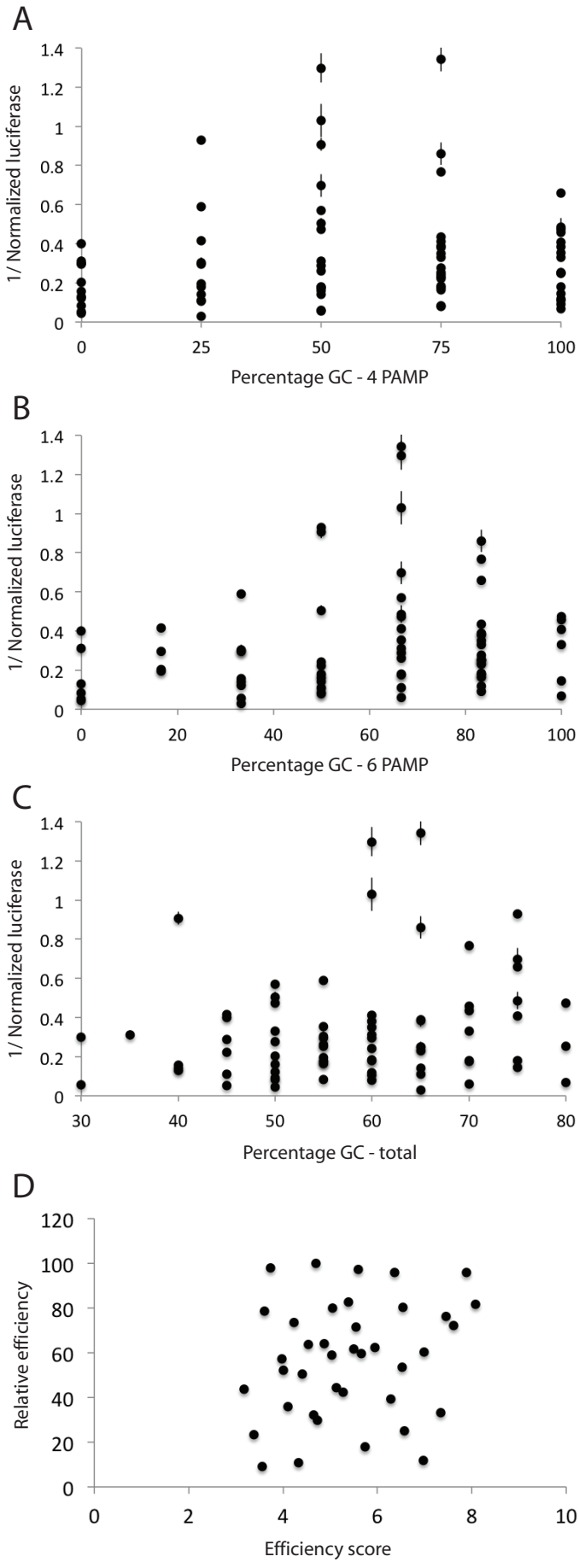
A
1/ Normalized luciferase
1.4
1.2
1
0.8
0.6
0.4
0.2
0
0
25
50
75
100
Percentage GC - 4 PAMP
B
1/ Normalized luciferase
1.4
1.2
1
0.8
0.6
0.4
0.2
0
0
20
40
60
80
100
Percentage GC - 6 PAMP
C
1/ Normalized luciferase
1.4
1.2
1
0.8
0.6
0.4
0.2
0
30
40
50
60
70
80
Percentage GC - total
D
Relative efficiency
120
100
80
60
40
20
0
0
2
4
6
8
10
Efficiency score

Figure S3: Analysis of GC content in relation to sgRNA efficiency

A-C: Comparison of sgRNA mutagenesis efficiency to GC content considering the final 4 nucleotides (A), the final 6 nucleotides (B) or the whole sgRNA sequence (C). **D:** Comparison of efficiency scores generated using the matrix shown in Figure 1B (horizontal axis) with efficiency (vertical axis) of sgRNAs published by Ren *et al.* (*16*).

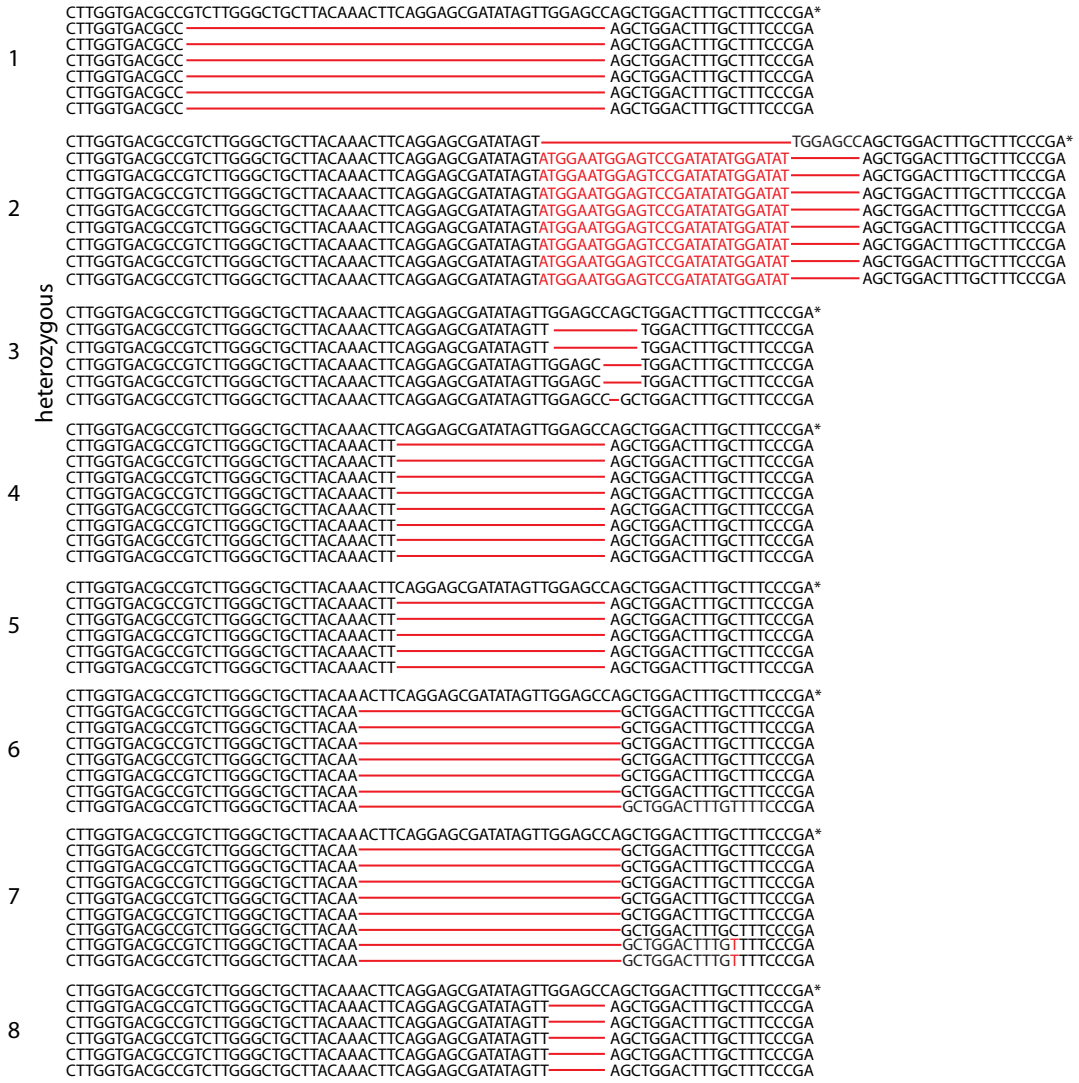

Figure S4: Sequencing of individual CRISPR mutant cells

Sequences are shown from 8 individual cells transfected with CRISPR reagents targeting the *yellow* gene. Samples are numbered 1 to 8, with a minimum of 5 sequence reads shown for each. The top row in each group shows wild-type sequence (marked with asterisks).

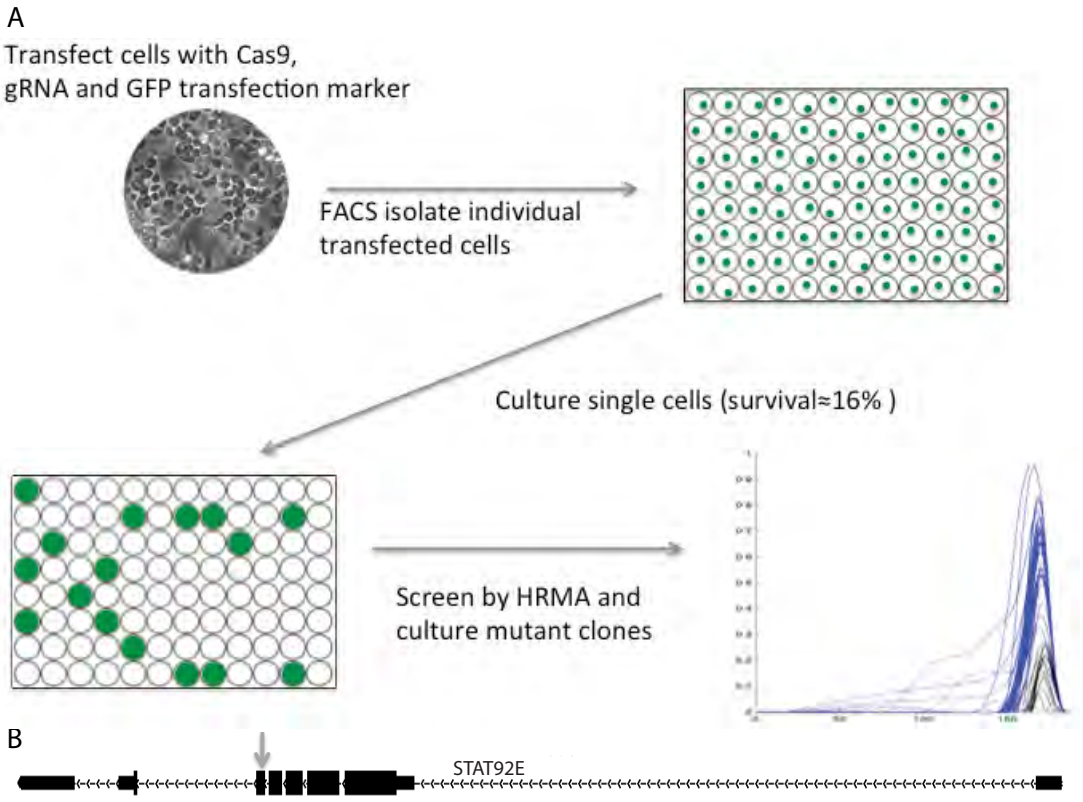

Figure S5: Generation of isogenic mutant cell lines

A: Workflow showing the major steps required to generate mutant cell lines.

B: Schematic of the *STAT92E* gene. UTRs are represented by thin black boxes, coding exons by thick black boxes and introns by black lines. Arrows superimposed on introns indicate the direction of transcription. CRISPR target site is shown by the grey arrow.

A

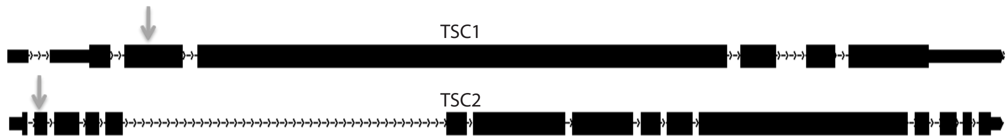

B TSC1

```
TGGAGGTACTGGTCAAAGCCCAGGCACCTCACGATGGGTACATCTTTGACAA*
TGGAGGTACTGGTCAAAGCCCAGGC-CCTCACGATGGGTACATCTTTGACAA
TGGAGGTACTGGTCAAAGCCCAGGC-CCTCACGATGGGTACATCTTTGACAA
TGGAGGTACTGGTCAAAGCCCAGGC-CCTCACGATGGGTACATCTTTGACAA
TGGAGGTACTGGTCAAAGCCCAGGC-CCTCACGATGGGTACATCTTTGACAA
TGGAGGTACTGGTCAAAGCCCAGGC-CCTCACGATGGGTACATCTTTGACAA
TGGAGGTACTGGTCAGTACCCAG———CTCACGATGGGTACATCTTTGACAA
TGGAGGTACTGGTCAGTACCCAG———CTCACGATGGGTACATCTTTGACAA
TGGAGGTACTGGTCAGTACCCAG———CTCACGATGGGTACATCTTTGACAA
TGGAGGTACTGGTCAGTACCCAG———CTCACGATGGGTACATCTTTGACAA
TGGAGGTACTGGTCAGTACCCAG———CTCACGATGGGTACATCTTTGACAA
```

```
TGGAGGTACTGGTCAAAGCCCAG————————————GCACCTCACGATGGGTACATCTTTGACAA*
TGGAGGTACTGGTCAAAGCCCAGTATGGG————————————CTCACGATGGGTACATCTTTGACAA
TGGAGGTACTGGTCAAAGCCCAGTATGGG————————————CTCACGATGGGTACATCTTTGACAA
TGGAGGTACTGGTCAAAGCCCAGTATGGG————————————CTCACGATGGGTACATCTTTGACAA
TGGAGGTACTGGTCAAAGCCCAGTATGGG————————————CTCACGATGGGTACATCTTTGACAA
TGGAGGTACTGGTCAAAGCCCAGGATGTACGTACAAAGC——————CCTCACGATGGGTACATCTTTGACAA
TGGAGGTACTGGTCAAAGCCCAGGATGTACGTACAAAGC——————CCTCACGATGGGTACATCTTTGACAA
TGGAGGTACTGGTCAAAGCCCAGGATGTACGTACAAAGC——————CCTCACGATGGGTACATCTTTGACAA
TGGAGGTACTGGTCAAAGCCCAGGATGTACGTACAAAGC——————CCTCACGATGGGTACATCTTTGACAA
TGGAGGTACTGGTCAAAGCCCAGGATGTACGTACAAAGC——————CCTCACGATGGGTACATCTTTGACAA
TGGAGGTACTGGTCAAAGCCCAGGATGTACGTACAAAGC——————CCTCACGATGGGTACATCTTTGACAA
TGGAGGTACTGGTCAAAGCCCAGGATGTACGTACAAAGC——————CCTCACGATGGGTACATCTTTGACAA
TGGAGGTACTGGTCAAAGCCCACTGGGGTACTTTGTACGTCCAGGATGG———ACGATGGGTACATCTTTGACAA
TGGAGGTACTGGTCAAAGCCCACTGGGGTACTTTGTACGTCCAGGATGG———ACGATGGGTACATCTTTGACAA
TGGAGGTACTGGTCAAAGCCCACTGGGGTACTTTGTACGTCCAGGATGG———ACGATGGGTACATCTTTGACAA
TGGAGGTACTGGTCAAAGCCCAGATGGTACAGCCCTGGATGTACCAAATGT——ACGATGGGTACATCTTTGACAA
TGGAGGTACTGGTCAAAGCCCAGATGGTACAGCCCTGGATGTACCAAATGT——ACGATGGGTACATCTTTGACAA
TGGAGGTACTGGTCAAAGCCCAGATGGTACAGCCCTGGATGTACCAAATGT——ACGATGGGTACATCTTTGACAA
TGGAGGTACTGGTCAAAGCCCAGATGGTACAGCCCTGGATGTACCAAATGT——ACGATGGGTACATCTTTGACAA
```

C TSC2

```
CAATTGGGATTCC-GGGATTCACAGGTTACGTGGGCGAGCGGACCCTGCGGCCGGAGTTTGAGAGGGAACTGCG*
CAATTGGGATTCCGGGGATTCACAGGTTACGTG————GGACCCTGCGGCCGGAGTTTGAGAGGGAACTGCG
CAATTGGGATTCCGGGGATTCACAGGTTACGTG————GGACCCTGCGGCCGGAGTTTGAGAGGGAACTGCG
CAATTGGGATTCCGGGGATTCACAGGTTACGTG————GGACCCTGCGGCCGGAGTTTGAGAGGGAACTGCG
CAATTGGGATTCCGGGGATTCACAGGTTACGTG————GGACCCTGCGGCCGGAGTTTGAGAGGGAACTGCG
CAATTGGGATTCCGGGGATTCACAGGTTACGTG————GGACCCTGCGGCCGGAGTTTGAGAGGGAACTGCG
CAATTGGGATTCCGGGGATTCACAGGTTACGTG————GGACCCTGCGGCCGGAGTTTGAGAGGGAACTGCG
CAATTGGGATTCCGGGGATTCACAGGTTACGTG————GGACCCTGCGGCCGGAGTTTGAGAGGGAACTGCG
CAATTGGGATTCCGGGGATTCACAGGTTACGTG————GGACCCTGCGGCCGGAGTTTGAGAGGGAACTGCG
CAATTGGGATTCCGGGGATTCACAGGTTACGTGG——GCGGACCCTGCGGCCGGAGTTTGAGAGGGAACTGCG
CAATTGGGATTCCGGGGATTCACAGGTTACGTGG——GCGGACCCTGCGGCCGGAGTTTGAGAGGGAACTGCG
CAATTGGGATTCCGGGGATTCACAGGTTACGTGG——GCGGACCCTGCGGCCGGAGTTTGAGAGGGAACTGCG
CAATTGGGATTCCGGGGATTCACAGGTTACGTGG——GCGGACCCTGCGGCCGGAGTTTGAGAGGGAACTGCG
CAATTGGGATTCCGGGGATTCACAGGTTACGTGG——GCGGACCCTGCGGCCGGAGTTTGAGAGGGAACTGCG
CAATTGGGATTCCGGGGATTCACAGGTTACGTGG——GCGGACCCTGCGGCCGGAGTTTGAGAGGGAACTGCG
CAATTGGGATTCCGGGGATTCACAGGTTACGTGG——GCGGACCCTGCGGCCGGAGTTTGAGAGGGAACTGCG
CAATTGGGATTCCGGGGATTCACAGGTTACGTGG——GCGGACCCTGCGGCCGGAGTTTGAGAGGGAACTGCG
CAATTGGGATTCCGGGGATTCACAGGTTACGTGG——GCGGACCCTGCGGCCGGAGTTTGAGAGGGAACTGCG
CAATTGGGATTCCGGGGATTCACAGGTTACGTGG——GCGGACCCTGCGGCCGGAGTTTGAGAGGGAACTGCG
CAATTGGGATTCCGGGGATTCACAGGTTACGTGG——GCGGACCCTGCGGCCGGAGTTTGAGAGGGAACTGCG
CAATTGGGATTCCGGGGATTCACAGGTTACGTGG——GCGGACCCTGCGGCCGGAGTTTGAGAGGGAACTGCG
```

Figure S6: Generation of *TSC1* and *TSC2* mutant cell lines

A: Schematics of the *TSC1* and *TSC2* genes. Details are as described for Figure S5A. **B-C:** Sequencing result for at least 20 clones from *TSC1* (B) or *TSC2* (C) mutant cell lines. Asterisks indicate wild-type sequence.

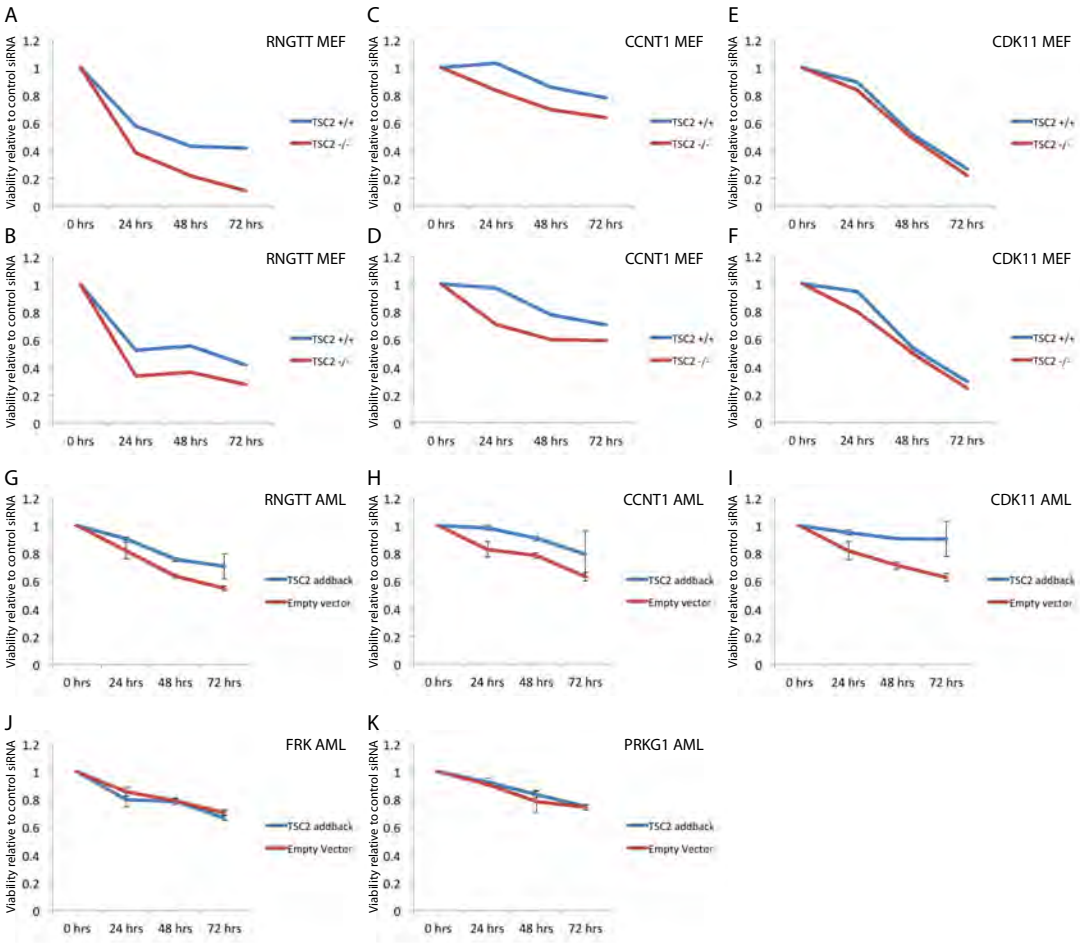

Figure S7: Synthetic effects in MEFs and AML cells

A-K: Viability plots over 72 hours relative to control siRNA treatments in wild type MEFs (A-F – blue lines), TSC2 deficient MEFs (A-F – red lines), AML cells (G-K – red lines) or AML cells with TSC2 addback (G-K – blue lines) treated with siRNA targeting the genes indicated. Results are from two biological replicates for MEFs (shown separately) and three biological replicates for AML cells. Error bars indicate standard error of the mean. See Figure 4C-D for summary plots of these data.

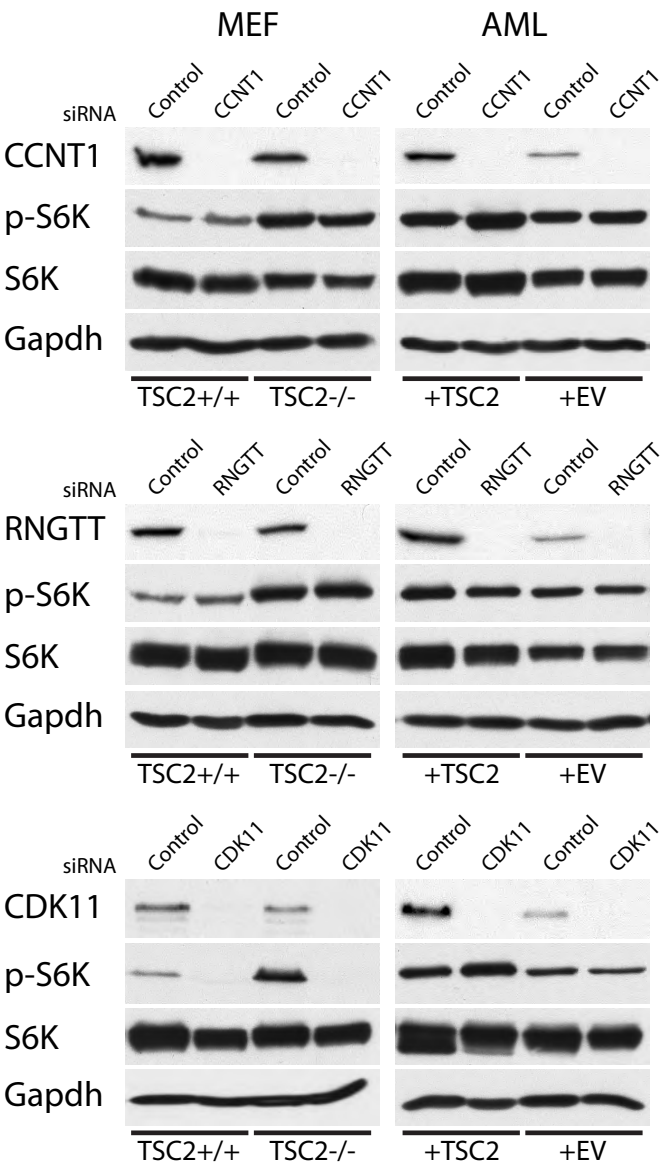

Figure S8: Analysis of knockdown of candidate genes on mTOR signaling

Western blots for the indicated proteins in wild-type MEFs (*TSC2*$^{+/+}$), TSC2 deficient MEFs (*TSC2*$^{-/-}$), AML cells (+EV) or AML cells with TSC2 addback (+TSC2) in the presence of siRNA targeting CCNT1, RNGTT or CDK11 as labeled. All Western Blots are representative of three biological replicates.

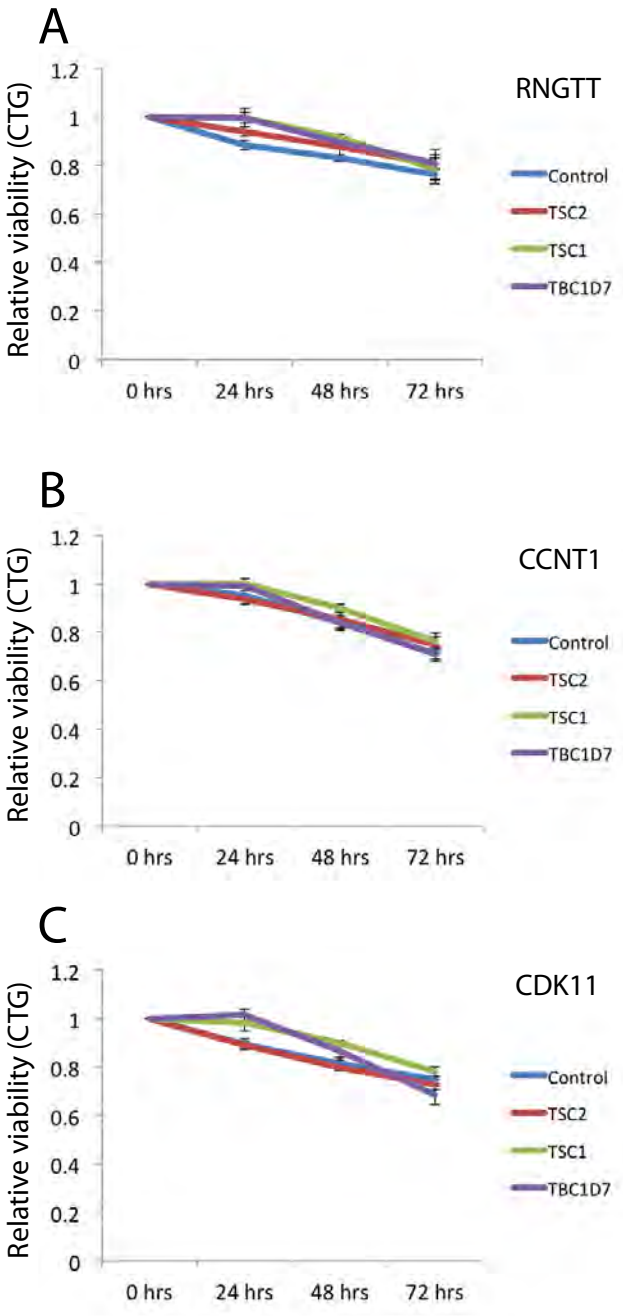

Figure S9: Synthetic effects of candidate genes with *TBC1D7*

A-C: Viability plots over 72 hours relative to control siRNA treatments in wild-type MEFs treated with siRNA targeting the genes indicated in combination with siRNA targeting *TSC1*, *TSC2* or *TBC1D7*. Results represent the average of three biological replicates and error bars indicate standard error of the mean.

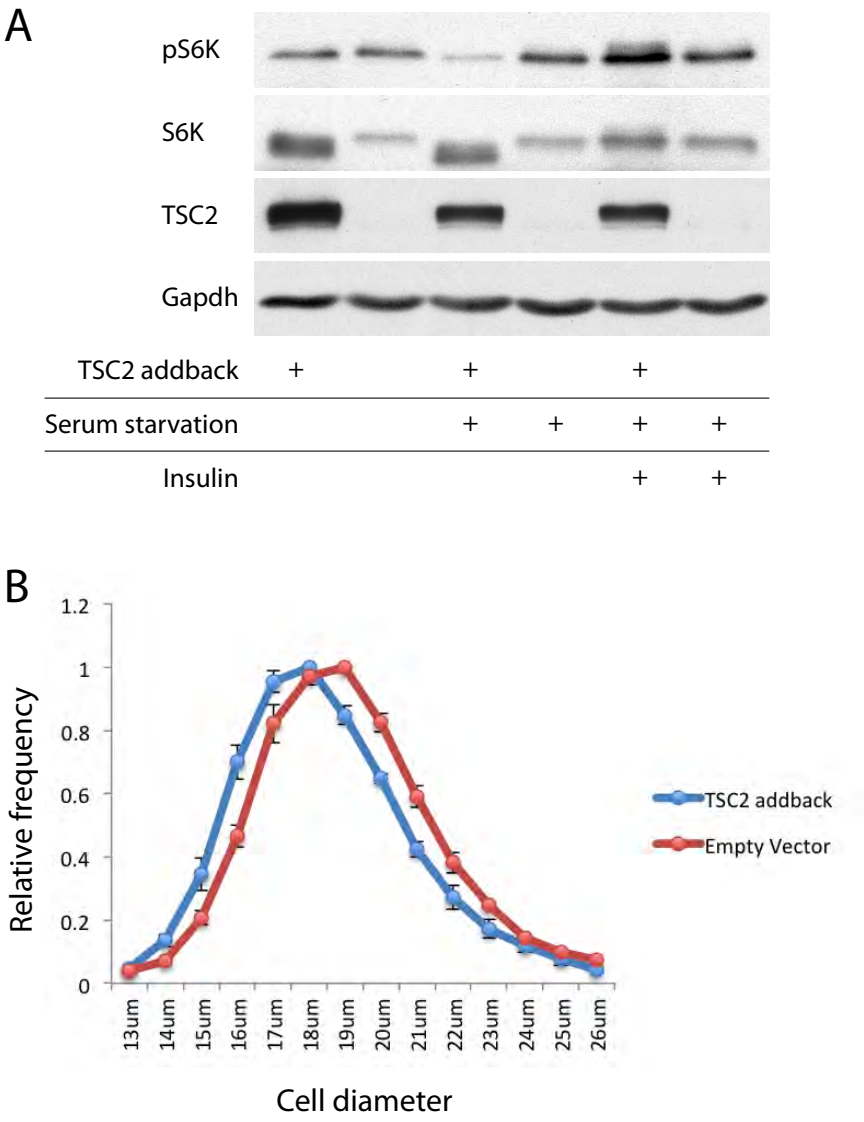

Figure S10: Analysis of TSC2 addback efficacy in AML cells

A: Western blots showing changes in p-S6K, total S6K, TSC2 or Gapdh in AML cells with or without TSC2 addback. Experiments were performed under standard culture conditions, serum starvation or with insulin stimulation as indicated. Westerns are representative of at least three biological replicates.

B: Plot showing the distribution of cell diameters of AML cells with (blue line) or without (red line) TSC2 addback. Results show the average from three biological replicates and error bars indicate standard error of the mean.